

¹ **GLO-Roots: an imaging platform enabling multidimensional characterization of soil-grown ~~roots~~root systems**

³ Rubén Rellán-Álvarez^{1, 9}, Guillaume Lobet², Heike Lindner^{1, 8}, Pierre-Luc Pradier^{1, 8, 10},
⁴ Jose Sebastian^{1, 8}, Muh-Ching Yee¹, Yu Geng^{1, 7}, Charlotte Trontin¹, Therese LaRue³,
⁵ Amanda Schrager-Lavelle⁴, Cara H. Haney⁵, Rita Nieu⁶, Julin Maloof⁴, John P. Vogel⁷, José
⁶ R. Dinneny^{1, 12}

⁷ ¹ Department of Plant Biology, Carnegie Institution for Science, Stanford, CA, USA.

⁸ ² PhytoSystems, University of Liège, Liège, Belgium.

⁹ ³ Department of Biology, Stanford University, Stanford, CA, USA.

¹⁰ ⁴ Department of Plant Biology, UC Davis, Davis, CA, USA.

¹¹ ⁵ Harvard Medical School, Massachusetts General Hospital, Department of Genetics, De-
¹² partment of Molecular Biology Boston, MA, USA

¹³ ⁶ USDA Western Regional Research Center, Albany, CA, USA

¹⁴ ⁷ DOE Joint Genome Institute, Walnut Creek, CA, USA

¹⁵ ⁸ These authors contributed equally

¹⁶ ⁹ Present address: Laboratorio Nacional de Genómica para la Biodiversidad (Langebio),
¹⁷ Unidad de Genómica Avanzada, Centro de Investigación y de Estudios Avanzados del Instituto
¹⁸ Politécnico Nacional (CINVESTAV-IPN), Irapuato, Guanajuato, México

¹⁹ ¹⁰ Present address: Boyce Thompson Institute for Plant Research/USDA, Ithaca, NY, USA.

²⁰ ¹¹ Present address: Energy Biosciences Institute, UC, Berkeley, CA, USA

²¹ ¹² Corresponding author

²² **Author contributions:**

²³ RR-A: Conception, design and development of the growth and imaging system and Arabidop-
²⁴ sis transgenic lines; acquisition, analysis and interpretation of data; drafting and revising the

25 article.

26 GL: Development of the GLO-RIA image analysis plugin, analysis and interpretation of data,
27 drafting and revising the article.

28 HL: Acquisition of data, development of the tomato growth and imaging setup.

29 P-LP: Acquisition of data, analysis and interpretation of data

30 JS: Development of Brachypodium transgenic lines, acquisition and analysis of Brachypodium,
31 Arabidopsis and tomato data.

32 MCY: Development of Arabidopsis and Brachypodium transgenic lines.

33 YG: Development of Arabidopsis transgenic lines.

34 CT: Acquisition and analysis of the QPCR data

35 TL: Acquisition and analysis of the QPCR data

36 AS-L: Contributed the unpublished dual-color tomato line.

37 CH: Contributed the unpublished *Pseudomonas fluorescens* CH267-lux strain.

38 RN: Contribution to the development of the Brachypodium transgenic line.

39 JM: Contributed the unpublished dual-color tomato line.

40 JPV: Contribution to the development of the Brachypodium transgenic line.

41 JRD: Conception, design and development of the growth and imaging system and Arabidopsis
42 transgenic lines; acquisition, analysis and interpretation of data; drafting and revising the
43 article.

44 All authors read and approve the final version of the manuscript.

45 **Abstract**

46 Root systems develop different root types that individually sense cues from their local
47 environment and integrate this information with systemic signals. This complex multi-
48 dimensional amalgam of inputs enables continuous adjustment of root growth rates, direction

49 and metabolic activity that define a dynamic physical network. Current methods for
50 analyzing root biology balance physiological relevance with imaging capability. To bridge
51 this divide, we developed an integrated imaging system called Growth and Luminescence
52 Observatory for Roots (GLO-Roots) that uses luminescence-based reporters to enable studies
53 of root architecture and gene expression patterns in soil-grown, light-shielded roots. We have
54 developed image analysis algorithms that allow the spatial integration of soil properties ~~such~~
55 ~~as soil moisture with root, gene expression and root system architecture~~ traits. We propose
56 GLO-Roots as a system that has great utility in presenting environmental stimuli to roots
57 in ways that evoke natural adaptive responses and in providing tools for studying the
58 multi-dimensional nature of such processes.

59 Introduction

60 Plant roots are three-dimensional assemblies of cells that coordinately monitor and acclimate
61 to soil environmental change by altering physiological and developmental processes through
62 cell-type and organ-specific regulatory mechanisms^{1,2}. Soil comprises a complex distribution
63 of particles of different size, composition and physical properties, airspaces, variation in
64 nutrient availability and microbial diversity^{3,4}. These physical, chemical and biological
65 properties of soil can vary on spatial scales of meters to microns, and on temporal scales
66 ranging from seasonal change to seconds. Root tips monitor this environment through locally
67 and systemically acting sensory mechanisms^{5,6}.

68 The architecture of the root system determines the volume of soil where resources can be
69 accessed by the plant (rhizosphere) and is under both environmental and genetic control.
70 Plasticity in growth parameters allows the plant to adjust its form to suit a particular soil.
71 Lateral roots, which usually make up the majority of the total root system, often grow at an
72 angle divergent from the gravity vector. This gravity set-point angle (GSA) is controlled by
73 auxin biosynthesis and signaling and can be regulated by developmental age and root type⁷.
74 Recent cloning of the *DRO1* Quantitative Trait Locus (QTL) demonstrates that natural
75 genetic variation is a powerful tool for uncovering such control mechanisms⁸.

76 Specific root ideotypes (idealized phenotypes) have been proposed to be optimal for acquisition
77 of water and nitrogen, which are distinct from ideotypes for low phosphorus. Based on
78 computational modeling and field studies, the “steep, deep and cheap” ideotype proposed by
79 Lynch and colleagues may provide advantages to the plant for capturing water and elements
80 like nitrogen that are water soluble and therefore tend to move in the soil column with water.
81 This ideotype consists of highly gravitropic, vertically oriented roots that grow deep in the
82 soil column and develop large amounts of aerenchyma, which reduces the overall metabolic
83 cost of the root system³. Other nutrients, like phosphorus, which have limited water solubility
84 and are tightly bound to organic matter, usually accumulate in the top layers of soil and favor
85 roots systems that are more highly branched and shallow. The low-phosphorus ideotype
86 effectively increases root exploration at the top layers of soil³. Modeling of root system
87 variables shows that optimum architecture for nitrogen and phosphorus uptake are not
88 the same⁹ and suggests tradeoffs that may affect the evolution of root architecture as a
89 population adapts to a particular environmental niche¹⁰.

90 Clearly, understanding the architecture of root systems and how environmental conditions
91 alter root developmental programs is important for understanding adaptive mechanisms
92 of plants and for identifying the molecular-genetic basis for different response programs.
93 In addition, roots systems have complexity beyond their architecture that needs to be
94 incorporated into our understanding of plant-environment interactions. Primary and lateral
95 roots exhibit different stress response programs in *Arabidopsis*^{2,11} and may play specialized
96 roles in water and nutrient uptake. Thus, it is important to develop methods that allow for
97 a multidimensional characterization of the root system that includes growth, signaling, and
98 interactions with other organisms. Furthermore, physiological parameters that affect whole
99 plant responses to the environment, such as transpiration, are likely integrated into such
100 processes, thus requiring a more holistic approach to studies of root function.

101 Based on these considerations we have developed a new root imaging platform, Growth
102 and Luminescence Observatory for Roots (GLO-Roots), which allows root architecture and
103 gene expression to be studied in soil-grown plants. GLO-Roots is an integrated system

104 composed of custom growth vessels, luminescent reporters and imaging systems. We use
105 rhizotrons that have soil volumes equivalent to small pots and support growth of Arabidopsis
106 from germination to senescence. To visualize roots, we designed plant-codon optimized
107 luciferase reporters that emit light of different wavelengths. To visualize reporter expression,
108 plants are watered with a dilute luciferin solution and imaged afterwards. We have built a
109 custom luminescence imaging system that automatically captures images of rhizotrons held
110 vertically. The signal from each reporter is distinguished using band-pass filters held in a
111 motorized filter wheel, which enables automated acquisition of images from plants expressing
112 both structural and environmentally and developmentally responsive reporters. We have
113 also developed GLO-RIA (GLO-Roots Image Analysis), an ImageJ¹⁰¹² plugin that allows
114 for automated determination of (among other traits) root system area, convex hull, depth,
115 width and directionality, which quantifies the angle of root segments with respect to gravity.
116 GLO-RIA is also able to relate root system parameters to local root-associated variables
117 such as reporter expression intensity and soil-moisture content.

118 Overall GLO-Roots has great utility in presenting environmental stimuli to roots in physio-
119 logically relevant ways and provides tools for characterizing responses to such stimuli at the
120 molecular level in whole adult root systems over broad time scales.

121 **Box 1.**

122 All resources for GLO-Roots, including the original raw data used in the manuscript, sample
123 images, GLO-RIA user manual, the latest software updates and the source code, can be
124 found at: <https://dinnenylab.wordpress.com/glo-roots/>

125 **Results.**

126 We have developed an integrated platform for growing, imaging and analyzing root growth
127 that provides advances in physiological relevance and retains the ability to visualize aspects
128 of root biology beyond structure.

¹²⁹ **The GLO-Roots ~~plattform~~platform.**

¹³⁰ GLO-Roots is comprised of four parts: i) growth vessels called rhizotrons that allow plant
¹³¹ growth in soil and root imaging; ii) luminescent reporters that allow various aspects of root
¹³² biology to be tracked in living plants; iii) GLO1 luminescence-imaging system designed to
¹³³ automatically image rhizotrons; iv) GLO-RIA, an image analysis suite designed to quantify
¹³⁴ root systems imaged using GLO-Roots.

¹³⁵ **Plant growth system.** GLO-Roots utilizes custom designed growth vessels classically
¹³⁶ known as rhizotrons, which hold a thin volume of soil between two sheets of polycarbonate
¹³⁷ plastic. Acrylic spacers provide a 2-mm space in which standard peat-based potting mix is
¹³⁸ added. Black vinyl sheets protect roots from light and rubber U-channels clamp the rhizotron
¹³⁹ materials together. Plastic racks hold the rhizotrons vertically and further protect the roots
¹⁴⁰ from light. Rhizotrons and rack are placed in a black tub and water ~~are~~is added, to a depth
¹⁴¹ of about 2 cm, at the bottom to maintain moisture in the rhizotrons during plant growth.
¹⁴² The volume of soil in the rhizotrons (100 cm^3) is similar to small pots commonly used for
¹⁴³ Arabidopsis and supports growth throughout the entire life cycle (Fig 1A-C and Supplement
¹⁴⁴ 1).

¹⁴⁵ To determine how the biology of plants grown in rhizotrons compares to other standard
¹⁴⁶ growth systems, we utilized high-throughput qRT-PCR to study how these conditions affect
¹⁴⁷ expression of 77 marker genes in root and shoot samples. These genes were curated from the
¹⁴⁸ literature and belong to a wide array of biological pathways including nutrient acquisition,
¹⁴⁹ hormone and light response and abiotic stress. Whole roots and shoot samples were collected
¹⁵⁰ at the end of the light and dark periods (Long-day conditions: 16 hour light, 8 hours dark)
¹⁵¹ from plants grown in rhizotrons, pots, and petri dishes with two different media compositions~~(~~1
¹⁵² 1X Murashige and Skoog basal salts (~~MS~~1~~ms~~) 1% sucrose or 0.25X ~~MS~~1~~ms~~, no sucrose
¹⁵³ (ms25). Principal component analysis of the gene expression values showed a separation of soil
¹⁵⁴ and gel-grown root systems in the the first principal components (Figure 1-figure supplement
¹⁵⁵ 1A). In roots grown on gel-based media, we observed enhanced expression of genes associated

156 with light-regulated pathways (flavonoid biosynthesis: *FLAVINOL SYNTHASE1*, *FLS1*,
157 *CHALCONE SYNTHASE*, *CHS* and photosynthesis: *RUBSICO SUBUNITS1A*~~RUBISCO~~
158 *SUBUNIT 1A*, *RBCS1A*, *CYCLOPHILIN 38*, *CYP38*), which is expected due to the
159 exposure of gel-grown roots to light. In addition, genes associated with phosphorus nutrition
160 (*LOW PHOSPHATE RESPONSE1*, *LPR1*, *PHOSPHATE STARVATION RESPONSE1*,
161 *PHR1*) were (Figure 1-figure table supplement 1) less expressed in soil-grown roots, suggesting
162 differences in nutrient availability between the different growth systems. Interestingly, shoot
163 samples where not ~~clearly distinguished~~as clearly separated by growth media and, instead,
164 time of day had a greater effect (Figure 1-Supplement 2). These data suggest root systems
165 may be particularly sensitive to media conditions and indicate that rhizotron-grown root
166 systems more closely approximate the biology of pot-grown plants than standard gel-based
167 media. Shoot weight and primary root length were significantly reduced for gel-grown plants
168 compared to rhizotron- or pot-grown plants suggesting significant differences in the biology
169 of plants grown under these conditions (Figure 1-figure supplement 1B-C).
170 While the 2 mm depth of the soil sheet is 10 to 20 times the average diameter of an Arabidopsis
171 root (between 100-200 microns⁴⁴¹³), we evaluated whether rhizotron-grown plants exhibited
172 any obvious stress as a consequence of physical constriction. We compared traits of plants
173 growing in vessels that hold similar volumes of soil but in different volumetric shapes. The
174 number of lateral roots was significantly lower in pot and cylinder-grown plants compared
175 to rhizotron-grown plants (Figure 1-figure supplement 1D) whereas primary root length of
176 rhizotron and cylinder-grown plants was significantly greater than pot-grown plants (Figure
177 1-figure supplement 1E). No significant differences in shoot area were observed between the
178 three systems (Figure 1-figure supplement 1-data). Thus, these data do not support the
179 hypothesis that rhizotron-grown plants experience physical constriction greater than other
180 vessels holding the same volume of soil.

181 **Generation of transgenic plants expressing different luciferases.** Arabidopsis roots
182 cannot easily be distinguished from soil using brightfield imaging due to their thinness and
183 translucency (Figure 1-figure supplement 3); thus, reporter genes are needed to enhance the

184 contrast between the root and their environment. Luciferase is an ideal reporter to visualize
185 roots: 1) unlike fluorescent reporters, luciferase does not require high-intensity excitation
186 light, which could influence root growth, 2) peat-based soil (a type of histosol) exhibits no
187 autoluminescence but does autofluoresce at certain excitation wavelengths similar to GFP
188 (Figure 1-figure supplement 3), 3) while GFP is very stable, and thus not as suitable for
189 imaging dynamic transcriptional events, the luciferase enzyme is inactivated after catabolism
190 of luciferin, making it ideal for studying processes such as environmental responses. A
191 considerable number of luciferases have been developed that emit light spanning different
192 regions of the visible spectrum, but their utilization has been limited to studies in animals
193 (Table 1).

194 To determine the efficacy of using luciferase to visualize roots in soil, we codon optimized
195 sequences of *PpyRE8*, *CBGRed*, *LUC2*, and *CBG99* for Arabidopsis expression. In addition,
196 nanoLUC¹⁴ and venus-LUC2⁴²¹⁵ were utilized. Constitutive luciferase expression was driven
197 in plants using the *UBIQUITIN 10* (*UBQ10*) or *ACTIN2* (*ACT2*) promoters using vectors
198 assembled through a Golden-Gate cloning system⁴²¹⁶. Plants homozygous for a single locus T-
199 DNA insertion were evaluated for in vivo emission spectra and luminescence intensity (Fig 1D).
200 All the evaluated luciferases use D-luciferin as a substrate facilitating the simultaneous imaging
201 of different luciferases except nanoLUC, which uses a proprietary substrate furimazine¹⁴. **In**
202 **general, luciferases Luciferases** with red-shifted emission spectra were less intense than the
203 green-shifted luciferases (Fig 1D). LUC2o showed an emission maximum at 580 nm and a
204 minor peak at 620 nm while CBG99o lacks the minor peak.

205 Continuous addition of luciferin did not have any significant effect on shoot weight or primary
206 root length (Figure 1-figure supplement 4). After luciferin addition, luminescence signal
207 could be reliably detected in root systems for up to 10 days, depending on the developmental
208 state of the plant.

209 **GLO1: a semi-automated luminescence imaging system for rhizotrons.** Lumines-
210 cence imaging systems commercially available for biomedical research are usually optimized

for imaging horizontally held specimens or samples in microtiter plates. Placing rhizotrons in this position would induce a gravitropic response in plants. Working with Bioimaging Solutions (San Diego, CA) we designed and built a luminescence imaging system optimized for rhizotron-grown plants. GLO1 (Growth and Luminescence Observatory 1) uses two PIXIS-XB back-thinned CCD cameras (Princeton Instruments, Trenton, NJ, USA) to capture partially-overlapping images of rhizotrons while a motorized stage automatically rotates the rhizotron to capture images of both sides (Fig 1E). A composite image is generated from the images captured of each side; Fig 1F shows that approximately half of the root system is revealed on each side with few roots being visible on both sides. Apparently, the soil sheet is thick enough to block portions of the root system but thin enough to ensure its continuous structure can be compiled from opposite face views. We tested the ability of GLO1-generated images to reveal complete root systems by manually quantifying the number of lateral roots in excavated root systems of 8 different plants and testing these results against estimates of lateral root number from images of the same plants visually inspected by 4 different persons. These comparisons revealed good correlation ($(R^2 = 0.974)$) between actual lateral root counts and image-based estimation, indicating GLO1-generated root images provide an accurate representation of the in soil root system.

GLO-RIA: GLO-Roots Image Analysis. We developed a set of image analysis algorithms that were well suited for the complex root systems that GLO-Roots is able to capture. GLO-RIA (Growth and Luminescence Observatory Root Image Analysis) is an ImageJ plugin divided in two modules. The first module (RootSystem) performs four different types of analysis: i) a local analysis that detects all root particles in the image and computes their position, length and direction; ii) the global analysis performs a root system level analysis and computes the total visible surface, convex hull, width and depth; iii) the shape analysis uses Elliptic Fourier Descriptors or pseudo-landmarks similarly to RootScape^{45,17} to perform a shape analysis on the root system iv) the directionality analysis computes the mean direction of root particles in a root system (either on the full image or by a user-defined region of interest in the image).

239 These four analysis methods are fully automated by default, but can be manually adjusted if
240 needed.

241 The second module of GLO-RIA (RootReporter) was specifically designed for the analysis of
242 multi-layered images such as combinations of gene reporter, root structure and soil moisture.
243 Shortly, the plugin works as follows: i) detection of the gene reporters and the structure
244 reporters in their respective images; ii) if needed, a manual correction can be performed to
245 correct the automated detection; iii) gene reporters are linked with the soil water content
246 and the structure reporters, based on their proximity; iv) gene reporter intensity (either
247 absolute or normalized using the structural reporter) is computed; v) all data are exported
248 and saved to a [RSML datafile](#)[Root System Markup Language \(RSML\) datafile¹⁶¹⁸](#). Gene
249 and structure reporters can be followed across different time and space points. Using
250 an object oriented approach, great care has been taken to facilitate the user interactions
251 on the different images to streamline the analysis process. Table 2 shows a list of root
252 system features extracted using GLO-RIA. GLO-RIA does not currently have the ability
253 to reconstruct the root architecture in itself (topological links between roots). This is a
254 challenge for analyzing images captured by GLO-Roots since soil particles cause disruption
255 of root segments.

256 [We tested the accuracy of the measurements obtained from GLO-RIA using two different](#)
257 [ground-truthed data sets. Manual measurement of root system width, depth and average](#)
258 [lateral root angle was determined by hand using imageJ from an independent set of images](#)
259 [corresponding to roots of several Arabidopsis accessions growing in control conditions. We](#)
260 [also used ArchiSimple¹⁹ to generate 1240 images of root system models with contrasting](#)
261 [sizes and lateral root angles. Since these images are computationally generated, exact](#)
262 [determination of root system parameters was possible. For both ground truth data sets,](#)
263 [GLO-RIA quantification provided measurements that were well correlated for all all](#)
264 [three measured parameters \(Figure 1-figure supplement 5D-F\). Sample images of real](#)
265 [and ArchiSimple generated root images are shown with GLO-RIA-defined directionality](#)
266 [color-coding \(Figure 1-figure supplement 5G-I\).](#)

267 Continuous imaging of root growth.

268 The size of our rhizotrons enables undisturbed root system development (before roots reach
269 the sides or the bottom of the rhizotron) for about 21-23 days for the Col-0 accession
270 growing under long day conditions (Figure 2); however root traits such as directionality
271 can be observed through later stages of plant development. See 35 DAS root system and
272 directionality in Figure 2A-B. An example of a time series spanning 11 to 21 days after
273 sowing (DAS) of Col-0 roots expressing *ProUBQ10:LUC2o* is shown in Fig 2A and [Video 1](#)
274 with a color-coded time projection shown in Fig 2C. Directionality analysis (Fig 2B) shows a
275 progressive change in root system angles from 0° - 0° (vertical) to 45° - 45° as lateral roots
276 take over as the predominant root type. Figure 2D shows the evolution over time of several
277 root traits that can be automatically captured by GLO-RIA (depth, width, area) and others
278 that were manually quantified (primary root growth rate or number of lateral roots per
279 primary root).

280 Root system architecture of different *Arabidopsis* accessions.

281 As a proof of concept to estimate the utility of our root imaging system to phenotype
282 adult root system traits, we transformed a small set of accessions (Bay-0, Col-0 and Sha)
283 with the *ProUBQ10:LUC2o* reporter and quantified RSA at 22 DAS (Fig 3A-C). GLO-RIA
284 analysis of these root systems identified several root traits that distinguish Col-0, Bay-0
285 and Sha. Directionality analysis revealed an abundance of steep-angle regions in the root
286 system of Bay while Sha showed an abundance of shallow-angled regions and Col-0 was
287 intermediate (Fig 3D). Bay-0 shows the deepest and narrowest root system leading to the
288 highest depth/width ratio while Sha has the widest root system (Fig 3E). Other root traits
289 such as root system area and the vertical center of mass also showed significant differences
290 (Figure 3-figure supplement 1B). Broad sense heritability values for depth (96.3), area (92.0),
291 depth/width (97.8), width (95.7) and vertical center of mass (95.0) were all higher than 90%.
292 To capture the richness of root architecture shape, we used GLO-RIA to extract pseudo-
293 landmarks describing the shape of the root system (see Materials and Methods for more

294 details) and performed PCA analysis. The first principal component captures differences in
295 the distribution of widths along the vertical axis and separates Col-0 and Sha from Bay-0
296 root systems. (Fig 3F). Bay-0 shows an homogenous distribution of widths along the vertical
297 axis while Sha and Col-0 are much wider at the top than bottom. PC2 seems to be capturing
298 a relationship between width at the top and total depth and separates Sha root systems
299 which are wide at the top and deep from Col-0 root systems which are wide but not as
300 deep as Sha. Shape information extracted from pseudo-landmarks can distinguish the three
301 different accession using PCA analysis (Fig 3G).[~](#)

302 **Spectrally distinct luciferases enable gene expression patterns, characterization**
303 **of root system interactions and microbial colonization.**

304 We tested whether spectrally distinct luciferase reporters would enable additional information
305 besides root architecture to be captured from root systems. Luciferase reporters have been
306 commonly used to study gene expression and these resources can potentially be utilized to
307 study such regulatory events in soil-grown roots. We transformed *ProACT2:PpyRE8o* into
308 two well studied LUC reporter lines: the auxin response reporter line *ProDR5:LUC*⁺¹⁷²⁰
309 (Figure A-B) and the Reactive Oxygen Species (ROS) response reporter *ProZAT12:LUC*⁺¹⁸²¹
310 (Figure 4C-D). We implemented in GLO-RIA an algorithm that semi-automatically identifies
311 gene reporter signal and associates this object to the corresponding root structure segment.
312 A graphical representation of the results obtained with Root Reporter can be observed in
313 Figure 4-figure supplement 1. Reporter intensity values along the first 5 mm of root tips can
314 also be observed in Figure 4-figure supplement 2.
315 We then took advantage of our ability to constitutively express two spectrally different
316 luciferases and imaged the overlapping root systems (one expressing *ProUBQ10:LUC2o* and
317 the other *ProACT2:PPy RE8o*). While two root systems were distinguishable using this
318 system (Figure 4-figure supplement 3); measurements of root system area did not reveal a
319 significant effect on root growth when two plants were grown in the same rhizotron, compared
320 to one; however, further studies are warranted (Figure 4-figure supplement 3).

321 The GLO-Roots system uses non-sterile growth conditions, which allows complex biotic
322 interactions that may affect responses to the environment. Bacteria themselves can be
323 engineered to express luminescent reporters through integration of the LUX operon, which
324 results in luminescence in the blue region of the spectrum and is thus compatible with the
325 plant-expressed luciferase isoforms we have tested. *Pseudomonas fluorescens* CH267¹⁹²²,
326 a natural *Arabidopsis* root commensal, was transformed with the bacterial LUX operon
327 and used to inoculate plants. Thirteen days after inoculation, we were able to observe
328 bacterial luminescence colocalizing with plant roots. *P. fluorescens* did not show an obvious
329 pattern of colonization at the root system scale level. As a proof-of-principle test of the
330 multi-dimensional capabilities of the GLO-Roots system we visualized both *LUC2o* and
331 *PPyRE8o* reporters in plants and the LUX reporter in bacteria in the same rhizotron (Figure
332 4-figure supplement 4).

333 **Adaptive changes in root system architecture under water deprivation, phos-**
334 **phorus deficiency and light.** To test the utility of the GLO-Roots system to understand
335 response of root systems to environmental stimuli we tested the effects of light and conditions
336 that mimic drought and nutritional deficiency. To examine the effects of light exposure on
337 the root architecture, the black shields, which normally protect the soil and roots from light,
338 were removed from the top half of the rhizotrons 10 DAS. Using directionality analysis we
339 detected a significant increase in the steepness of roots only in the light exposed region of
340 the rhizotron, while the lower shielded region showed no difference. (Fig 6-figure supplement
341 3A-B and Fig 6-figure supplement 4). Light can penetrate the top layers of soil²⁰²³ and it
342 has been proposed to have a role in directing root growth specially in dry soils²¹²⁴ through
343 the blue light receptor *phot1*. Root directionality was not significantly different between light
344 and dark-treated roots of the *phot1/2* double mutant suggesting that blue light perception
345 is necessary for this response^{2124,2225} (Fig 6-figure supplement 3B-lower panel). These
346 data highlight the strong effects of light on root system architecture²³²⁶, which GLO-Roots
347 rhizotrons are able to mitigate.

348 Plants grown in low-P soil showed a significant increase in the width-depth ratio of the root

349 system compared to plants grown in P-replete soil, as determined using the automated root
350 system area finder in GLO-RIA (Fig 6-figure supplement 2A-B). Plants under P deficiency
351 showed an increase in the ratio between root-shoot area (Fig 6-figure supplement 2C) and
352 higher investment of resources in the development of the root system at the expense of
353 shoot growth (Fig 6-figure supplement 2D). Root systems of control and P-deficient plants
354 showed no significant differences in directionality at 22 DAS but at 27 DAS, roots were more
355 horizontally oriented in P-deficient plants (Fig 6-figure supplement 2E). The observed changes
356 in root architecture are consistent with root system ideotypes that improve phosphorus
357 uptake efficiency.

358 GLO-Roots is especially well suited for studying water-deficit (WD) responses. First, shoots
359 are exposed to the atmosphere and vapor pressure deficit (**VPD**) is maintained at levels that
360 allow for transpiration of water from the shoot. Second, soil in rhizotrons is exposed to
361 air at the top and dries **basipetally** (from the top-down); drying soil increases the volume
362 occupied by air and reduces contact of root with liquid water, all of which are similar to
363 changes in soil expected in the field during WD. Finally, as peat-based soil dries, its optical
364 properties change, allowing moisture content to be approximated from bright-field images.
365 We took advantage of the change in gray-scale pixel intensity to construct a calibration
366 curve (Figure 5-figure supplement 1) that quantitatively relates gray-scale pixel intensity to
367 moisture content (Fig 5A); water content can be color coded in images with appropriate look
368 up tables (Fig 5B). Soil color was not affected by the presence or absence of roots (Figure
369 5-figure supplement 2). Using this approach, water content in a rhizotron can be mapped
370 and visualized in 2D (Fig 5C-D). In the example shown, we can observe that a 22 DAS Bay-0
371 plant depleted soil-moisture content locally around the **the** root system (Figure 5E).

372 We performed several trials to simulate WD in our growth system. Plants were germinated,
373 grown under control conditions then transferred to 29°C and standing water removed from
374 the container holding the rhizotrons starting at 9 DAS or 13 DAS. Elevated temperature
375 combined with water deficit is a common stress that modern crops varieties are poorly
376 adapted to, thus highlighting the importance of examining this combined treatment^{24,27,25,28}.

377 Plants were maintained in this WD regime until 22 DAS when luciferin solution was added
378 and the plants imaged. At 13 DAS, lateral roots near the soil surface are already emerged
379 ([Video 1](#), Figure 2A) and 9 days of subsequent WD treatment caused lateral roots to show an
380 increase in gravitropism leading to the development of a root system that were deeper and
381 more vertically oriented (Fig 6A). Roots of Bay-0 plants showed similar responses, though
382 the extent of change was less pronounced since Bay-0 roots are normally more vertically
383 oriented (Fig 6B). Plants transferred at 9 DAS and grown for 13 days under WD showed less
384 lateral root development in the top layer of soil (Fig 6E). At this time point, lateral roots
385 start to emerge ([Video 1](#)) and early drought may lead to growth quiescence or senescence.
386 Careful examination of roots in these regions showed evidence of small lateral root primordia
387 populating the primary root (Figure 6F). After 24 h of re-watering (Figure 6G) these lateral
388 root primordia reinitiated growth (Figure 6H).

389 Time-lapse imaging of the water deficit response showed that changes in root growth direction
390 occurred ahead of the dry soil front [Video 2](#). Using GLO-RIA we were able correlate local
391 water moisture contents with the orientation of root segments. With this approach we
392 observed that root segments in dryer areas of rhizotron grew at steeper root angles (Figure
393 7) than roots in WW regions, though lateral root angle in wetter regions was also affected.
394 These data suggest that both local and systemic signaling is likely involved in redirecting
395 lateral roots deeper during the simulated drought treatments tested here.

396 We also grew plants under WD at control temperatures or under WW conditions at elevated
397 temperature to test the effects of these individual stresses on root architecture. We observed
398 that both conditions were sufficient to induce a change in root directionality indicating that
399 the plant uses similar mechanisms to avoid heat and water-deficit associated stresses (Figure
400 6-figure supplement 1). We next asked which regulatory pathways controlled the observed
401 changes in lateral root directionality during simulated drought. Hydrotropism is a known
402 environmental response that directs root growth towards wet regions of soil. MIZ1 is an
403 essential regulator of hydrotropism; however *miz1* mutants had no significant effect on water
404 deficit-induced changes in root directionality, compared to wild type (Fig 6C), indicating

405 that this response was distinct from hydrotropism. Auxin is an important mediator of
406 gravitropism and auxin treatment causes lateral roots to grow more vertically⁷. Consistent
407 with this role for auxin, mutant plants with loss of function in the auxin receptor TIR1, did
408 not show changes in the root system directionality between WW and WD conditions (Fig
409 6D).

410 **GLO-Roots for Brachypodium and Tomato.**

411 To examine the general applicability of the GLO-Roots system for other species, we introduced
412 LUC2o-expressing reporters into the model grass *Brachypodium distachyon* and the crop
413 plant *Lycopersicon esculentum* (tomato). Brachypodium is well suited to the GLO-Root
414 system because, like Arabidopsis, its small size allows mature root systems to be studied in
415 relatively small soil volumes^{2629,2730}. *LUC2o* driven by the *ZmUb1* promoter was introduced
416 into Brachypodium using the pANIC vector²⁸³¹. Brachypodium roots showed a distinct
417 architecture from Arabidopsis marked by prolific development of secondary and tertiary
418 lateral roots (Fig 8A). This is consistent with other studies that show that Brachypodium
419 has a typical grass root system²⁷³⁰. Comparison of root system development in rhizotrons
420 with gel-based media showed that root growth is higher in soil than in plates (Figure 8-figure
421 supplement 1). Previous work has suggested that auxin levels in Brachypodium roots is sub-
422 optimal for growth²⁹³². Pacheco-Villalobos and colleagues suggest that, in Brachypodium,
423 and contrary to what happens in Arabidopsis, ethylene represses *YUCCA* reducing the
424 synthesis of auxin. The reduced growth that we observe in plates and the high levels of
425 ethylene that build up in sealed plates³⁰³³ would support this mechanism.

426 Tomato plants were transformed with *Pro35S:PPyRE8o* and *ProeDR5rev:LUC2* reporters.
427 The plants showed more rapid growth than Arabidopsis or Brachypodium and required
428 fertilizer to prevent obvious signs of stress (reduced growth, anthocyanin accumulation).
429 Root systems were imaged from 17 DAS plants. Roots showed presumptive lateral root
430 primordia marked by DR5-expression (Fig 8C-D). These results show that the GLO-Roots
431 method can be applied to study root systems of plants and will likely be useful for studying

432 root systems of other small to medium sized model plants and for early stages of larger crop
433 plants.

434 **Discussion.**

435 **GLO-Roots enables a multi-dimensional understanding of root biology.**

436 Recent studies of root systems has emphasized structural attributes as important contributors
437 of root system function. Indeed, studies examining the role of genetic variants in tolerating
438 abiotic stress have demonstrated the importance of such characteristics⁸. Roots, however,
439 are highly diverse in the biology they perform and a multi-dimensional understanding of root
440 systems, which incorporates differences in signaling, metabolism and microbial association
441 as well as structure, may provide a clearer understanding of the degree to which sub-
442 functionalization of the root system plays a role in important processes such as acclimation
443 and efficient resource acquisition.

444 We have developed tools in GLO-Roots that allow for tracking multiple aspects of soil
445 physicochemical properties and root biology simultaneously. Using GLO-Roots, we are able
446 to map in 2D coordinates soil physical properties such soil moisture together with root
447 architecture traits such as directionality, growth rates and gene expression levels. All this
448 information is aggregated in layers for each x, y coordinate. Using GLO-RIA we integrate this
449 multilayer information, leveraging our ability to simultaneously and seamlessly investigate
450 root responses to environmental stimuli such as soil moisture content. **Luciferase isoforms**
451 **Luciferases** that emit light at different wavelengths allow for constitutive and regulated
452 promoters to be studied together. Introduction of luciferase reporters into microbes provides
453 an additional layer of information that provides a readout on the association between
454 organisms and how this might be affected by environmental conditions. The flexibility
455 of the GLO-Roots system may enable additional dimensionality to our understanding of
456 root biology. Other physical properties such as CO₂ or pH mapping in rhizotrons have
457 already been enabled by using planar optodes^{34,35}. It may be possible to engineer LUX-based

458 reporters in microbes that are responsive to extracellular metabolites, creating microbial
459 biosensors, and integration of such tools may enable root-exudation and nutrition to be
460 analyzed in soil. Split-Luciferase reporters have been engineered that allow bi-molecular
461 interactions to be studied. Finally, molecular sensors analogous to FRET sensors, termed
462 BRET-sensors³²³⁵, may allow metabolite tracking dynamically through the root system.
463 With additional innovation in the development of luciferase reporters, the GLO-Roots systems
464 will likely expand the repertoire of biological processes that can be studied over an expanded
465 range of developmental time points and environmental conditions.

466 **Enhanced root growth and gravitropism may constitute an avoidance mechanism
467 used during water deficit stress.**

468 It has been proposed that plants with steep root systems will be better able to tap into deep
469 water resources and thus perform better under water deprivation. For example in rice, the
470 IR64 paddy cultivar shows shallow root systems in upland fields whereas Kinandang Patong,
471 an upland cultivar, is deeper rooting⁸. Plants maintain a number of regulatory pathways
472 that mediate changes in physiology during WD. Enhanced growth of root systems has been
473 well characterized in field-grown plants; however this has not been recapitulated in studies of
474 gel-grown Arabidopsis plants. Thus, it has been unclear whether Arabidopsis simply responds
475 to WD differently. Our results here show that Arabidopsis does indeed maintain a classical
476 WD response that expands the root system and directs growth downward. Interestingly,
477 under our stress regime, we did not observe a significant decrease in the relative water
478 content of shoot tissues (Figure 6-figure supplement 5), suggesting that the changes in root
479 architecture were sufficient to provide access to deep water and prevent dehydration. Such
480 changes in root growth are likely regulated through systemic and local signaling that involve
481 auxin signaling but acts independently of known pathways that control moisture-directed
482 root growth.

483 Perspectives and Conclusions.

484 Understanding plant biology requires a sophisticated understanding of how environmental
485 stimuli affect the form and function of plants as well as an understanding of how physiological
486 context informs such responses. Environmental conditions are at least as complex as the
487 plants they affect. Plant roots are exposed to a variety of environmental signals that change
488 in time and space at very different scales that are integrated at the whole plant system. It is
489 an important challenge in biology to develop methods of growing and studying plants that
490 present such stimuli in a manner that the plant is likely to encounter in nature. After all, the
491 plants we study have evolved to survive through mechanisms that have been selected, over
492 evolutionary time, in nature. It will be interesting for future studies to determine how other
493 environmental stimuli affect root growth using GLO-Roots and whether these responses
494 differ between accessions of Arabidopsis. Identification of the genetic loci responsible for
495 phenotypic variation in adult root phenotypes may identify the molecular basis for adaptive
496 variation that exists in this species and potentially identify loci that are useful for breeding
497 efforts needed for the next green revolution.

498 Materials and methods.

499 Growth system.

500 **Rhizotrons and growth system fabrication.** Rhizotrons are composed of two sheets of
501 1/8" abrasion resistant polycarbonate plastic (Makrolon AR (R)) cut to size using a water
502 jet (AquaJet LLC, Salem, OR), two acrylic spacers cut using a laser (Stanford Product
503 Realization Lab), two rubber U-channels cut to strips 30 cm long ([McMaster Carr part #](#)
504 [8507K33](#)) and two sheets of black 0.030" thick polypropylene sheets ([McMaster Carr part #](#)
505 [1451T21](#)) cut with a straight-edge razor blade. Rhizotron designs were drafted in Adobe
506 Illustrator (Adobe, San José, CA). The blueprints of all the parts are provided in Supplement
507 1. The top edge of each polycarbonate sheet was painted with black 270 Stiletto nail polish
508 (Revlon, New York, NY).

509 **Boxes and holders.** Rhizotrons are held vertical during plant growth in a custom rack
510 system composed of two sheets of 1/4" black acrylic plastic cut with slots for eleven rhizotrons
511 using a laser, four 3/8" PVC rods ([McMaster Carr part # 98871a041](#)) secured with PVC
512 nuts ([McMaster Carr part # 94806a031](#)) to hold the acrylic sheets horizontal. The rack is
513 placed inside a 12" x 12" x 12" black polyethylene tank ([Plastic Mart part # R121212A](#)).

514 **Rhizotron preparation** The procedure to construct a rhizotron with soil is as follows:
515 Two pieces of polycarbonate plastic are laid flat on a table with the spacers inserted. Using
516 an electric paint gun, a fine mist of water is applied to the bare polycarbonate sheets. Then,
517 using a 2 mm sieve (US Standard Sieve Series N° 10) a fine layer of PRO-MIX(r) PGX soil
518 (Premier Tech, Canada) is applied. Excess soil is discarded by gently tapping the plastic
519 against the table in a vertical position. Water is sprayed again onto the soil, then a second
520 layer of Pro-MIX is applied as before. For P deficiency experiments soil supplemented with 1
521 ml of 100 µM P-Alumina (control) and 0-P-Alumina (P deficient) was used. To prevent the
522 soil from falling out of the bottom opening, a 3 x 6 cm piece of nylon mesh is rolled into a 1
523 cm wide tube and placed at the bottom side of the rhizotron. The spacers are removed and
524 replaced by clean spacers. The two faces of the rhizotron are carefully joined together and
525 two rubber U-channels slipped on to clamp all pieces together. Assembled rhizotrons are
526 placed into the rack inside the boxes and 500 mL of water is added to the box.

527 **Plant growth** *Arabidopsis thaliana* seeds were stratified for 2 d at 4 °C in Eppendorf tubes
528 with distilled water. Seeds were suspended in 0.1 % agar and 5 to 10 were sown using a
529 transfer pipette in the rhizotron. A transparent acrylic sheet was mounted on top of the box
530 and sealed with tape to ensure high humidity conditions that enable *Arabidopsis* germination.
531 Three days after sowing, the cover was unsealed to decrease humidity and allow the seedlings
532 to acclimate to a dryer environment. From 3 days after sowing (DAS) to the time the first
533 true leaves emerged, it was critical to ensure that the top part of the rhizotron remained
534 humid for proper germination of the plants. Between three and five DAS the rhizotrons
535 were thinned leaving only the number plants required for that experiment, typically one,
536 except for experiments examining root-root interactions. Unless otherwise stated, all the

537 experiments presented here, treatments were started 10 DAS. Plants were grown under long
538 day conditions (16 h light / 8 h dark) using 20–22 °C (day/night) and 150 µE m⁻¹ s⁻¹. Two
539 types of growth environments were used for experiments. A walk-in growth chamber with
540 fluorescent lightning and a growth cabinet with white LED lights. Relative water content
541 measurements were done as previously described³³³⁶

542 **qRT-PCR analysis.**

543 Seeds were surface sterilized as described before² and grown in rhizotrons, 100 cm³ pots, or
544 on two types of 1% agar (Duchefa) media containing either 1x MS nutrients (Caisson) and 1%
545 Sucrose, (termed ms media) or ¼x MS nutrients only (termed ms25 media). Both media were
546 buffered using 0.5 g/L MES and pH was adjusted to 5.7 with KOH. All plants were grown
547 together in a growth cabinet with LED lights under long day conditions (16h day/8h night).
548 Root and shoot tissue was collected separately from individual plants at the end of the day
549 (1 hour before the lights shut off) and at the end of the night (1 hour before lights came on).
550 Three biological replicates were collected for each condition. RNA was extracted using the
551 Plant RNA MiniPrepTM kit (ZYMO Research) according to manufacturer's instructions
552 with on-column DNase treatment (Qiagen). cDNA was made using the iScript Advanced
553 cDNA Synthesis for RT-qPCR kit (Bio-Rad) from 200 ng of total RNA. qRT-PCR was
554 performed using a Fluidigm BioMarkTM 96.96 Dynamic Array IFC with the EvaGreen®
555 (Bio-Rad) fluorescence probe according to the Fluidigm Advanced Development Protocol
556 number 37. For the analysis, all the reactions with no amplification (Ct = 999) were set to
557 the maximal Ct for that assay type. The two technical replicates were then averaged and
558 dCt values calculated using AT3G07480, AT4G37830, At1g13320 and At1g13440 as reference
559 internal controls. PCA plots were generated with Devium Web³⁴³⁷ using dCt values. dCT
560 values were calculated as dCT = CT~gene interest~ - mean(CT~reference gene~). Primers
561 used are listed in file Supplement 8.

562 **Biological components.**

563 **Codon optimization of luciferases.** The following luciferases that emit light at different
564 wavelengths were codon optimized for Arabidopsis (Genscript, Piscataway, NJ): LUC2: a
565 yellow improved version (Promega, Madison, WI) of the original *Photinus pyralis* (firefly)
566 LUC.

- 567 • Ppy RE8: a red variant³⁵³⁸ of the *P. pyralis* thermostable variant Ppy RE-TS³⁶³⁹.
- 568 • CBG99: a green variant (Promega, Madison, WI) from yellow click beetle (*Pyrophorus*
569 *plagiophthalmus*) luciferases.
- 570 • CBR: a red variant (Promega, Madison, WI) from yellow click beetle.

571 **Non-optimized luciferases.** We also used the following non-optimized luciferases:

- 572 • nanoLUC: a blue luciferase isolated from a deep sea shrimp¹⁴.
- 573 • venusLUC2: a venus-LUC2 fusion reported to show higher luminescence output than
574 LUC2⁴²⁴⁵.
- 575 • A transposon containing the bacterial luciferase-containing LUX operon was integrated
576 into the *Pseudomonas fluorescens* CH267¹⁹²² genome by conjugation with *E. coli*
577 *SM10pir* containing pUT-EM7-LUX³⁷⁴⁰ and used to track root microbe colonization.
578 For inoculation 9 DAS plants were inoculated with 2 mL of an overnight bacterial
579 culture resuspended in 10 mM MgSO₄ and diluted to 0.01 OD.

580 **Generation of single-reporter transgenic plants.** We generated transcriptional fu-
581 sions of all luciferases to constitutive promoters to examine the activity level and emission
582 spectrum of each isoform. The *attL1-attL2* entry clones containing plant-codon optimized
583 coding sequence of *LUC2*, *PpyRe8*, *CBG99* and *CBR* were synthesized by Genscript. A
584 DNA fragment including the *UBQ10* promoter region and first intron was amplified from
585 Col-0 genomic DNA with primers incorporating the attB1, attB4 combination sites at the
586 5' and 3' respectively. The PCR product was then introduced into pDONRTM P4-P1R

587 (Invitrogen) through a classic Gateway BP-reaction. The resulting plasmid, the *attL1*-*attL2*
588 entry clones with luciferase sequences, an empty *attR2*-*attL3** entry clone and the destination
589 vector dpGreenmCherry² were used to construct *ProUBQ10:LUC2o*, *ProUBQ10:PpyRE8o*,
590 *ProUBQ10:CBG99o* and *ProUBQ10:CBRo* through Gateway LR reactions. The destination
591 vector *dpGreenmCherry* contains a plasma membrane-localized mCherry coding sequence
592 driven by the 35S promoter and is used as a selectable marker of transformation at the
593 mature seed stage². We used Golden Gate cloning and the destination vectors that we had
594 generated before⁴³¹⁶ for the following fusions: *ProUBQ10:nanoLUC2*, *ProUBQ10:venusLUC*,
595 *ProACT2:PpyRE8o*. Briefly, the different components of each construct were PCR amplified
596 with complementary BsaI or SapI cutting sites, mixed with the destination vector in a single
597 tube, digested with either BsaI or SapI, ligated with T4 DNA ligase, then transformed
598 into E. coli Top10 cells and plated on LB antibiotic plates containing X-gal as previously
599 described⁴³¹⁶. Junction sites were confirmed by sequencing. We used pSE7 (Addgene
600 ID #: pGoldenGate-SE7: 47676) as the destination vector of the *ProUBQ10:nanoLUC2*,
601 *ProUBQ10:venusLUC* constructs and pMYC2 (Addgene ID #: pGoldenGate-MCY2: 47679)
602 as the destination vector for *ProACT2:PpyRE8o*. Maps of all the vectors can be found in
603 Supplement 8. *ProUBQ10:LUC2o* was transformed into Col-0, Bay and Sha accessions, the
604 *tir1-1*³⁸⁴¹ mutant and the *miz1*³⁹⁴² T-DNA insertion line (SALK_126928).

605 **Brachypodium distachyon.** The Arabidopsis plant-codon optimized Luciferase gene,
606 *LUC2o*, was inserted into the monocot vector pANIC10 via Gateway cloning²⁸³¹. *Brachy-*
607 *podium distachyon* plants were transformed using the method of Vogel and Hill⁴⁰⁴³.

608 **Tomato.** The transcriptional fusion *ProeDR5:LUC2* was generated by cloning the
609 *ProeDR5:LUC2* DNA fragment into the pBIB expression vector via restriction sites SalI
610 and Acc65I. The eDR5 promoter is an enhanced version of DR5 containing 13 repeats of
611 the 11-nucleotide core DR5 element⁴⁴⁴⁴ and the pBIB expression vector contains an NPTII
612 resistance gene under the control of the NOS promoter for use as a selectable marker during
613 transformation. All tomato transformations were performed by the Ralph M. Parsons

614 Foundation Plant Transformation Facility (University of California, Davis).

615 **Generation of dual-reporter plants.** To generate dual-reporter plants expressing lu-
616 ciferase isoforms that emit light with divergent emission spectra we used *ProACT2:PpyRE8o*
617 as the root structural marker and ZAT12:LUC¹⁸²¹ and DR5:LUC+¹⁷²⁰ lines that were
618 transformed with the *ProACT2:PpyRE8o* construct. All constructs were transformed using
619 a modified floral dip method as described in².

620 To make the dual color tomato plants, the *Pro35S:PpyRE8o* transcriptional fusion was
621 generated by putting the plant-codon optimized coding sequence described above into
622 the pMDC32 expression vector through a Gateway LR reaction. The pMDC32 vector
623 contains a hygromycin resistance gene under the control of the 35S promoter for use as a
624 selectable marker during transformation. This construct was transformed into the transgenic
625 *ProeDR5:LUC2* tomato line.

626 **In vivo emission spectra of plants constitutively expressing luciferase isoforms.**

627 To generate *in vivo* emission spectra of all constitutively expressed luciferases, seeds were
628 sterilized and sown on MS plates as described before². After 8 days, seedlings were treated
629 with a 100 µM luciferin solution, incubated at room temperature for 3 hours and imaged using
630 an IVIS Spectrum imaging system (Perkin Elmer, Waltham , MA) using 20 nm band-pass
631 emission filters at the following wavelengths (in nm: 490-510, 510-530, 530-550, 550-570,
632 570-590, 590-610, 610-630, 630-650, 650-670, 670-690, 690-710). Raw images were analyzed
633 using Fiji and *in vivo* emission spectra were constructed. The full emission spectra of LUX
634 and nanoLUC could not be constructed since the maximum of these two luciferases is below
635 the lower band pass filter that were available.

636 **Imaging system.** We designed a custom imaging system (GLO1, Growth and Lumines-
637 cence Observatory 1) optimized for imaging dual-reporter luciferase expression in our custom
638 rhizotrons. The design was a joint effort with Bioimaging Solutions (San Diego, CA) who
639 also built the system and wrote the acquisition software that drives all the mechanical parts

640 of the system. The system is composed by two 2048 x 2048 PIXIS-XB cameras (Princeton
641 Instruments, Trenton, NJ) mounted on top of each other to capture two fields of view
642 encompassing approximately two 15 x 15 cm areas corresponding to the top or bottom of
643 the rhizotron. The cameras are fitted with a Carl-Zeiss macro lens. A filter wheel with space
644 for four, 76.2 mm filters is positioned in front of the cameras and controlled by a stepper
645 motor allowing for automated changing of the filter wheel position. We used two -542/50
646 and 450/70- custom cut Brightline(R) band-pass filters (Semrock, Rochester, NY). In single
647 color imaging mode, the filter wheel is operated without filters. Positioned in front of the
648 filter wheel is a removable rhizotron holder mounted on a stepper motor. This stepper motor
649 is also controlled by the GLO-1 software allowing automatic acquisition of images from both
650 sides of the rhizotron sequentially. The whole imaging system is enclosed in a light-tight
651 black box with a door that allows loading and un-loading of rhizotrons.

652 **Plant Imaging.** Around 50 mL of 300 μ M D-luciferin (Biosynth, Itasca, IL) was added to
653 soil at the top of the rhizotron. In general 5 min exposures were taken per rhizotron, per
654 side, per channel. For daily imaging experiments, plants were imaged at dawn (+/- 1 hr)
655 to reduce possible effects on diurnal rhythms of keeping plants in the dark during imaging.
656 Shoot images were taken using a Nikon D3100 camera.

657 **Image Preparation.** Four individual images are collected: top front, bottom front, top
658 back and bottom back. Using an automated [ImageJ macro](#), a composite image is generated
659 as follows: 1)To correct for differences in background values between the two cameras the
660 mean background value of each image is subtracted from 200; 2) images are rotated and
661 translated to control for small misalignments between the two cameras; 3) the top and
662 bottom images of each side are merged; 4) the back image is flipped horizontally; 5) the
663 front and back images are combined using the maximum values. When dual color images are
664 acquired this operation is repeated for each channel. The final images produced are 16-bit
665 depth and 4096 x 2048 pixels. The scale of the images is 138.6 pixels per cm. Considering
666 that an *Arabidopsis* roots is 100 μ m this results in 1.39 pixels across an *Arabidopsis* root.

667 **GLO-RIA imageJ plug-in.** GLO-RIA uses a combination of existing tools to extract
668 relevant root architecture features. Directionality is acquired using the [directionality plugin](#)
669 from ImageJ. After the number of direction bins (we usually use bins of $2\frac{9}{2}^o$) is defined by
670 the user, a 5x5 sobel operator is used to derive the local gradient orientation. This orientation
671 is then used to build a distribution of directions by assigning the square of the orientation
672 into the appropriate bin. Instead of representing the total counts at each orientation a
673 relative value is calculated by dividing the individual values at each bin by the total sum
674 of the histogram (and multiplying by 100). Similar algorithms have been used to quantify
675 dynamic changes in the plant cytoskeleton⁴²⁴⁵.

676 The Elliptic Fourier Descriptors are aquired using the [Fourier Shape Analysis plugin](#) on
677 convex hull shape of the root system. Elliptic Fourier Descriptors have been used in numerous
678 studies to analyse variations in shapes, notably in leaves (e.g.⁴³⁴⁶).

679 The shape analysis is inspired by RootScape⁴⁵¹⁷. Due to the absence of fixed, recognisable
680 structures in root system (that are required for the position of true landmarks), pseudo-
681 landmarks are automatically extracted from the root systems. Shortly, the image is divided
682 vertically at equidistant positions (with the number defined by the user) and for each of the
683 image stripes, the minimum and maximum x coordinates are computed. The shape analysis
684 is therefore able to discriminate root system with different vertical root distributions or
685 global root system orientation (e.g. chemotropism) . The code source for the plugin, manual
686 and sample images can be found in the [github repository](#) of the project.

687 Statistical analysis was performed in R⁴⁵⁴⁸. The tidyR⁴⁶⁴⁹, dplyr⁴⁶⁴⁹, gridExtra⁴⁷⁵⁰,
688 shapes⁴⁸⁵¹, geomorph⁴⁹⁵², ggplot2⁵⁰⁵³ and cowplot⁵¹⁵⁴ packages were used for data
689 preparation, analysis and plotting. Final figure preparation was done in Inkscape.

690 **Data availability.** All the scripts and original data used to analyze and produce the images
691 can be accessed in the Github repository of the project: github.com/rr-lab/GLO-Roots. Raw
692 files of all the images used in the paper are availabe in [Dryad](#).

₆₉₃ **Acknowledgements.**

₆₉₄ Work in the lab of JRD was funded by the Carnegie Institution for Science Endowment and
₆₉₅ grants from the National Science Foundation (MCB-115795) and Department of Energy,
₆₉₆ Biological and Environmental Research program (DE-SC0008769). RRA was supported by a
₆₉₇ Carnegie Postdoc Fellowship and currently by Conacyt Ciencia Básica Joven Investigador
₆₉₈ grant number (CB-2014-01-238101). GL was supported by the Belgian Fonds de la Recherche
₆₉₉ Scientifique. JM was funded by the National Science Foundation (IOS-0820854). CH is
₇₀₀ funded by MGH Toteston & Fund for Medical Discovery Fellowship grant 2014A051303
₇₀₁ and NIH R37 grant GM48707 and NSF grant MCB-0519898 awarded to Frederick Ausubel,
₇₀₂ and previously by the Gordon and Betty Moore Foundation through Grant GBMF 2550.01
₇₀₃ from the Life Sciences Research Foundation. JV was funded by the Office of Biological and
₇₀₄ Environmental Research, Office of Science, US Department of Energy, interagency agreements
₇₀₅ DE-SC0001526 and DE-AI02-07ER64452. We thank Robert Mittler and Philip Benfey for
₇₀₆ providing seeds of ZAT12:LUC and DR5:LUC+ respectively.
₇₀₇ We also thank Neil Robbins and members of the Dinneny lab for critical review of the
₇₀₈ manuscript and suggestions during the development of the project. We greatly appreciate
₇₀₉ Tim Doyle at the Stanford Small Animal Imaging Facility for providing ~~'s advice in using~~
₇₁₀ ~~and help with advice in the use of~~ luciferase-based imaging approaches.

₇₁₁ **Competing interests.**

₇₁₂ We do not have any competing interests that we are aware of.

₇₁₃ **Tables**

⁷¹⁴ **Tables.**

⁷¹⁵ **Table 1:** Luciferases used in this study.

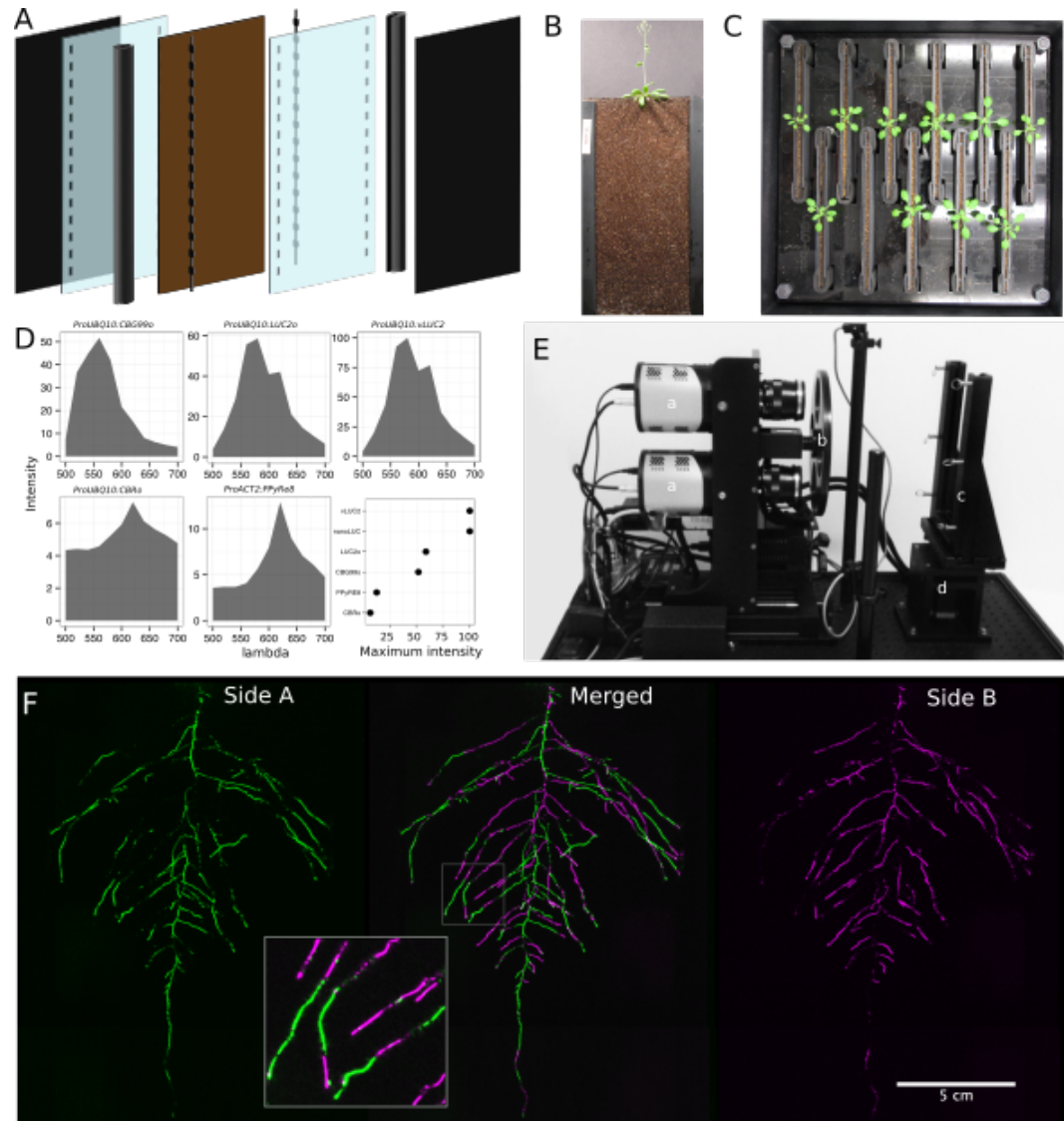
Luciferase	Origin	maximum wavelength	Substrate
Ppy RE8	firefly	618	D-luciferin
CBGRed	click beetle	615	D-luciferin
venus-LUC2	FP + firefly	580	D-luciferin
LUC(+)	firefly	578	D-luciferin
CBG99	click beetle	537	D-luciferin
lux operon	A. fischeri	490	biosynthesis pathway encoded within operon
nanoLUC	Deep sea shrimp	470	furimazine

⁷¹⁶ **Table 2:** list of root system features extracted using GLO-RIA.

variable	unit
projected area	cm^2
number of visible roots	-
depth	cm
width	cm
convex hull area	cm^2
width	cm
feret	cm
feret angle	°
circularity	-
roundness	-
solidity	-
center of mass	cm
Directionality	°
Euclidean Fourier Descriptors	-

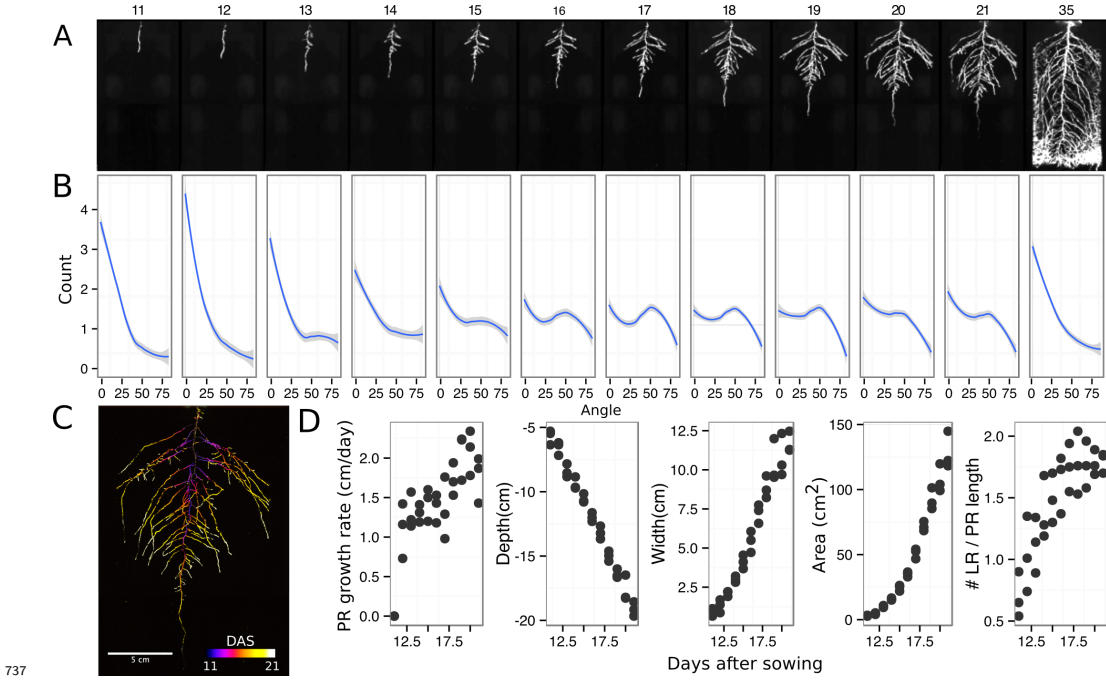
variable	unit
Pseudo landmarks	-

717 **Figures**

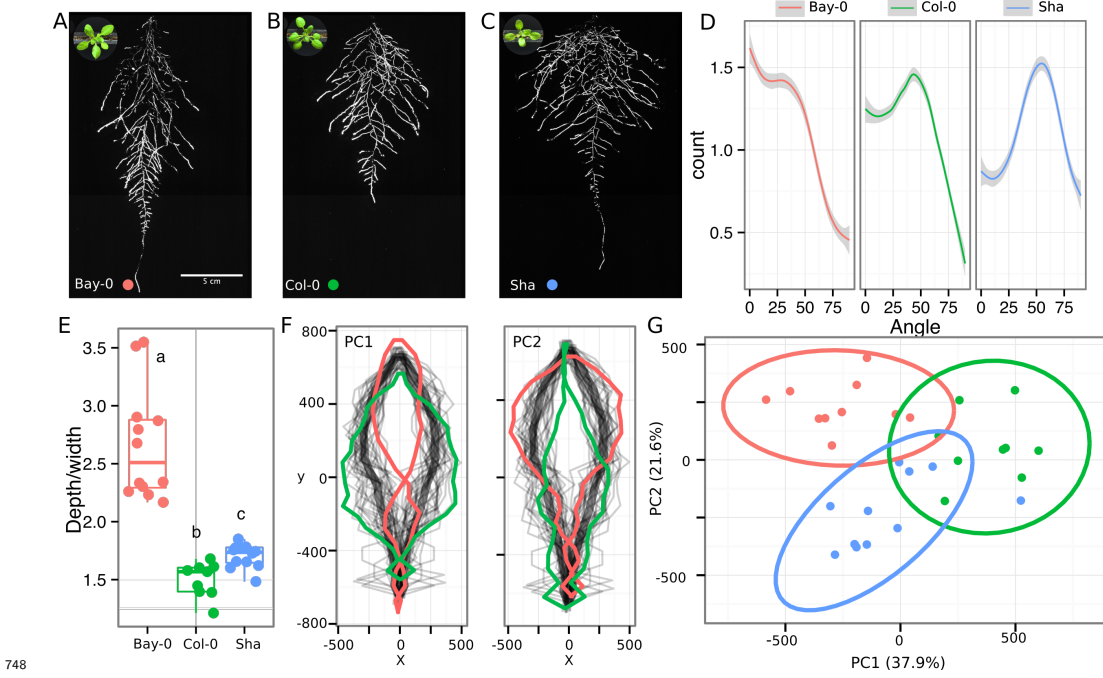


718 **Figure 1. GLO-Roots growth and imaging systems** A) 3D representation of the
 719 different physical components of the rhizotron: plastic covers, polycarbonate sheets,
 720 spacers and rubber U-channels. Blueprints are provided in Supplementary material 1. In brown, soil
 721 layer. B) Thirty five day-old plant in rhizotron with black covers removed. C) Top view
 722 of holding box with eleven rhizotrons. D)In vivo emission spectra of different luciferases
 723 used in this study. Transgenic homozygous lines expressing the indicated transgenes were
 724

725 grown on agar media for 8 days. Luciferin (300 μ M) was sprayed on the seedlings and plates
726 were kept in the dark and then imaged for 2 s at wavelengths ranging from 500 to 700 nm.
727 Five intensity values were taken from different parts of the roots of different seedlings and
728 averaged. Relative maximum intensity values are indicated in the lower right graph. E)
729 GLO 1 imaging system. The system is composed by two back illuminated CCD cameras
730 (a) cooled down to -55 °C. A filter wheel (b) allows for spectral separation of the different
731 luciferases. On the right, a rhizotron holder (c) is used to position the rhizotrons in front of
732 the cameras. A stepper motor (d) rotates the rhizotron 180° to image both sides. F) A 21
733 DAS plant expressing *ProUBQ10:LUC2o* was imaged on each of two sides of the rhizotron;
734 luminescence signal is colorized in green or magenta to indicate side. In the middle of the
735 panel, a combined image of the two sides is shown. The inset shows a magnified part of the
736 root system. FW: fresh weight, PR: Primary root.

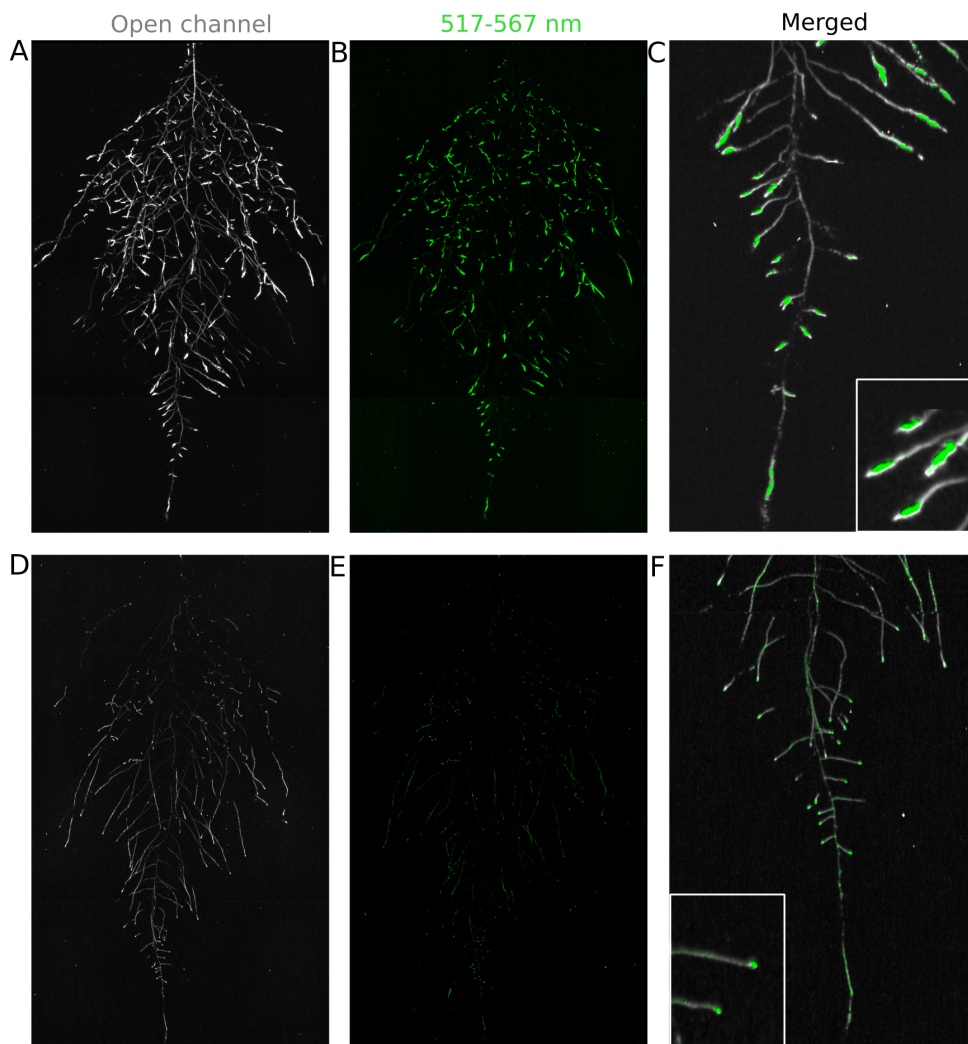


738 **Figure 2. Time-lapse imaging of root systems and quantification using GLO-**
 739 **RIA.** A) Typical daily time-lapse image series from 11 to 35 DAS of a *ProUBQ10:LUC2o*
 740 Col-0 plant. B) Directionality of the root system of plants in panel A calculated using the
 741 directionality plugin implemented in GLO-RIA. C) Color coded projection of root growth
 742 using the images in panel A. D) Primary root growth rate, depth, width, root system area
 743 are automatically calculated from the convex hull, which is semi-automatically determined
 744 with GLO-RIA. Lateral root number and number of lateral roots divided by the primary
 745 root length were quantified manually. A Local Polynomial Regression Fitting with 95%
 746 confidence interval (grey) was used to represent the directionality distribution curve. (0° is
 747 the direction of the gravity vector).



749 **Figure 3. Variation in root architecture between accessions of *Arabidopsis*.**

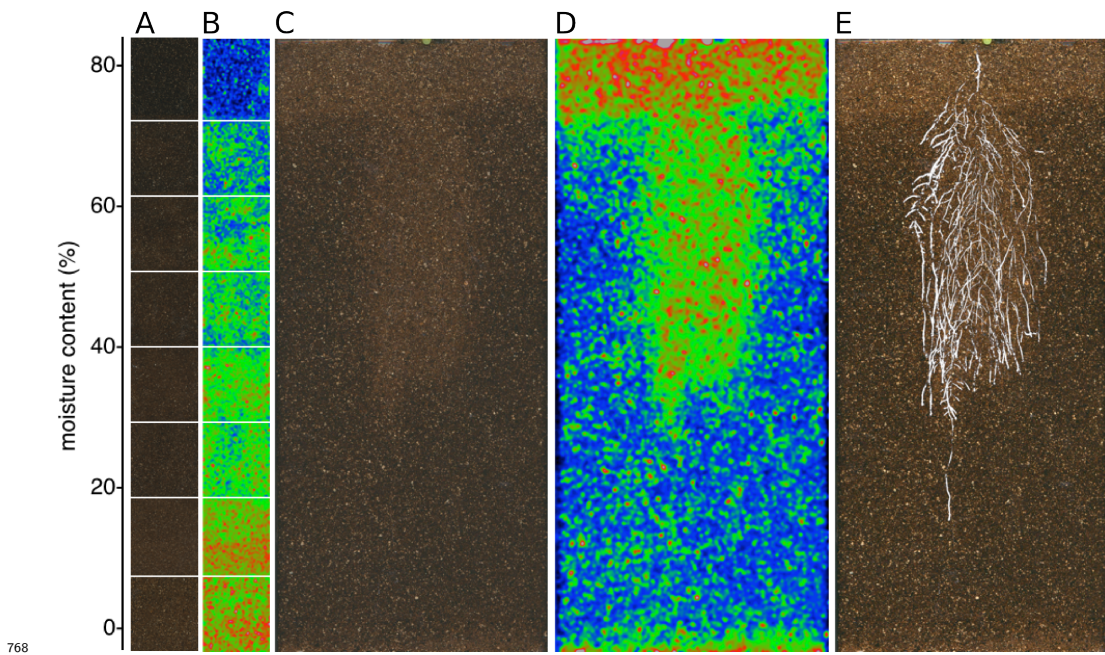
750 Representative root and shoot images of A) Bay-0, B) Col-0 and C) Sha accessions transformed
 751 with `_ProUBQ10:LUC2o_` and imaged after 22 DAS. D) Directionality of the root systems,
 752 E) depth/width ratio, F) Pseudo-landmarks describing shape variation in root system
 753 architecture. Eigenvalues derived from the analysis of 9-12 plants per accession is shown.
 754 The first two Principal Components explaining 38% (PC1) and 22% (PC2) of the shape
 755 variation are plotted. PC1 captures homogeneity of root system width along the vertical axis
 756 and PC2 a combination of depth and width in top parts of the root system. Red and green
 757 lines indicate -3SD and +3SD (Standard Deviations), respectively G) PC separation of the
 758 different ecotypes using the PCs described in (F). A Local Polynomial Regression Fitting
 759 with 95% confidence interval (grey) was used to represent the directionality distribution
 760 curve. 0° is the direction of the gravity vector. Wilcoxon test analysis with p < 0.01 was
 761 used to test significant differences between the different accession (n = 9-12 plants).



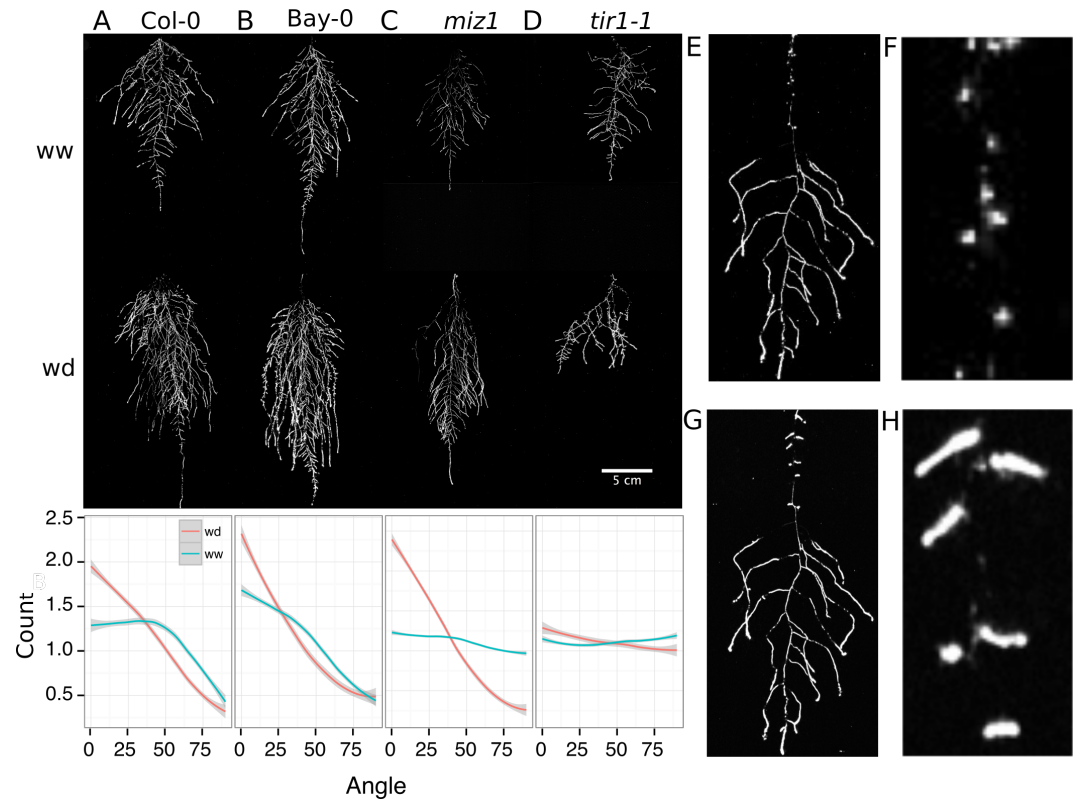
762

763 **Figure 4. Dual-color reporter visualization of structure and gene expression.**

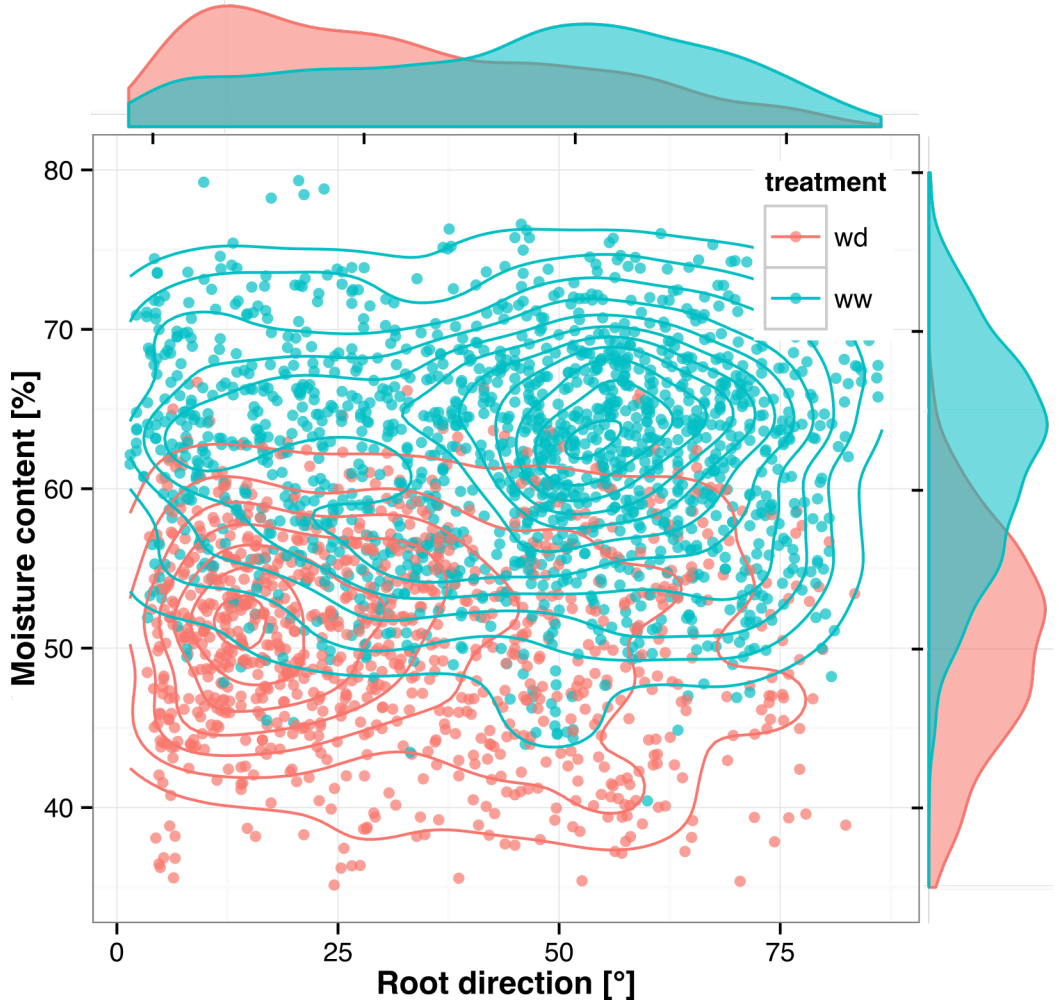
764 Images of whole root systems (A, D) or magnified portion of roots (C, F) at 22 DAS
 765 expressing *ProDR5rev:LUC+* (green, A, B) or *ProZAT12:LUC* signal (green, D, E) with
 766 skeletonized representation of roots generated using the *ProACT2:PpyRE8o* reporter
 767 expression (in grey).



769 **Figure 5. Soil moisture and root architecture mapping in rhizotrons.** A) Com-
 770 posite image showing regions of soil made from rhizotrons prepared with different moisture
 771 levels. B) Differences in grey-scale intensity values were enhanced using a 16-color Look Up
 772 Table (LUT). Brightfield image of soil in rhizotron (C) and converted using 16-color LUT to
 773 enhance visualization of distribution of moisture (D) . E) Root system of a Bay-0 22 DAS
 774 and subjected to water deprivation since 13 DAS. Root system visualized using luminescence
 775 and overlaid on brightfield image of soil in (C).



776 **Figure 6. Study of effect of water deficit on root system architecture.** A-D)
 777 Root systems 22 DAS and exposed to water deficit 13 DAS onwards. Sample images of
 778 well watered (left panels) and water deficit (right panels) root systems treated from 13
 779 DAS and directionality (line graphs to left of images) for (A) Col-0 (B) Bay-0 (C) *miz1*
 780 mutant and (D) *tir1-1*. E) Root system of a 22 DAS plant exposed to water deprivation
 781 from 9 DAS onwards with magnified view of lateral root primordia (F). G) The same
 782 root as in (E) 24 hours after rewetting and magnified view of lateral root primordia (H).
 783 Kolmogorov-Smirnov test at $p < 0.001$ was used to compare directionality distributions
 784 between the different treatments and genotypes. A Local Polynomial Regression Fitting
 785 with 95% confidence interval (grey) was used to represent the directionality distribution
 786 curve. 0° is the direction of the gravity vector.
 787



788

789 **Figure 7. Relationship between local soil moisture content and root growth**
 790 **direction.** Data quantified from the time lapse series shown in [Video 2](#). Density plots shown
 791 at periphery of graph for root direction (x-axis) and soil moisture (y-axis). 0° is the direction
 792 of the gravity vector. Data represents 2535 root tips measured in a series encompassing 10
 793 time points.

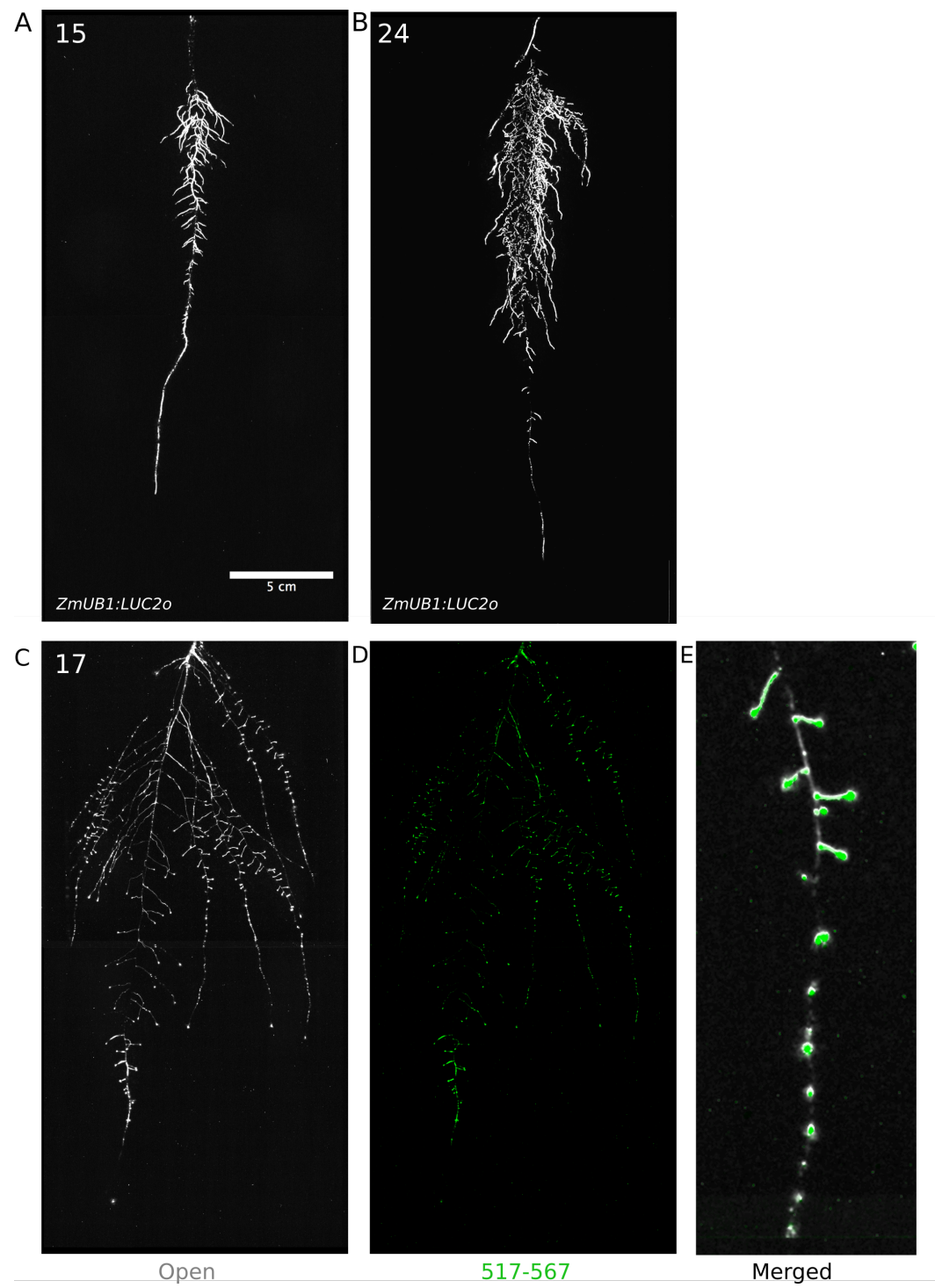


Figure 8: Roots of *Brachypodium distachyon* transformed with *ProZmUB1:LUC2o* and

⁷⁹⁶ imaged at 15 (A) and 24 (B) DAS grown in control conditions. C) Open channel of 17 DAS
⁷⁹⁷ tomato plant transformed with *ProeDR5rev:LUC2o* and *Pro35S:PPyRE8o* D) Green channel
⁷⁹⁸ showing only *ProeDR5rev:LUC2o* E) Amplification of the open and green channel showing
⁷⁹⁹ increased expression of *ProeDR5rev:LUC2o* reporter in early-stage lateral roots.

800 **Videos**

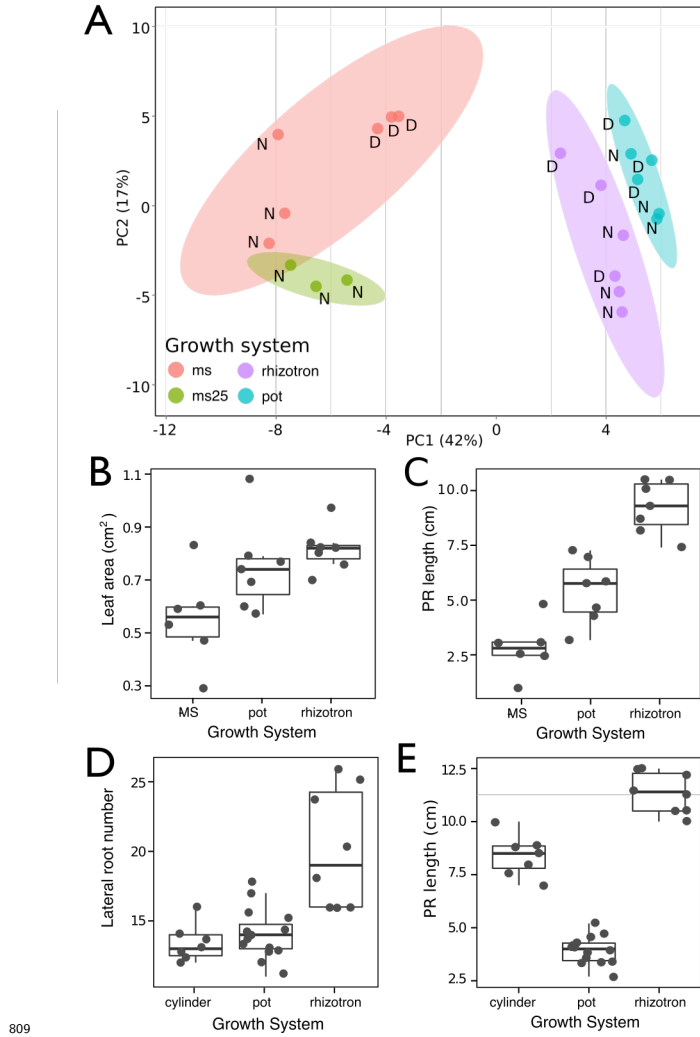
801 **Video 1** Time lapse from 11 to 21 DAS of a Col-0 plant expressing ProUBQ10:LUC2o
802 grown in control conditions

803 **Video 2** Time lapse from 16 to 24 DAS of Col-0 plants expressing *ProUBQ10:LUC2o*
804 growing in water deficient (left) and control (right) conditions. Plants were sown under
805 control conditions and water deficit treatment started 11 DAS. Images were taken every day.

806 

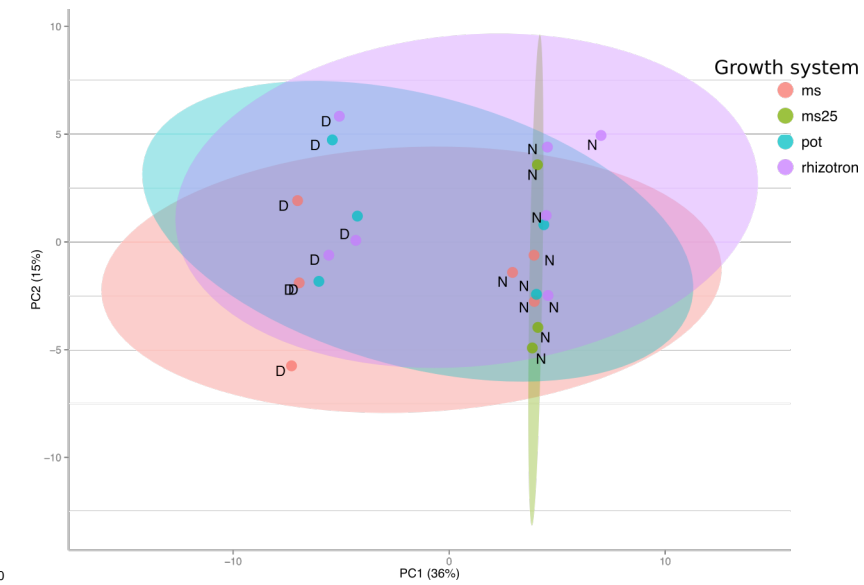
807 **Supplementary Material**

808 **Supplementary figures**



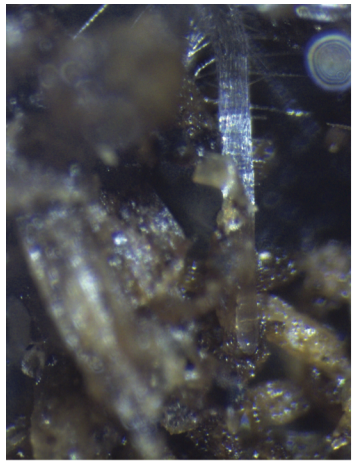
809
810 **Figure 1-figure supplement 1. Effect of different growth systems on plant biol-**
811 **ogy.** A) Principal Components Analysis (PCA) score plot of a set of 76 genes analyzed by
812 qPCR from root samples of plants grown in MS plates, pots, and rhizotrons. After 15 DAS
813 three plants were collected at the end of the day (D) and three were collected at the end of
814 the night (N). (ms = plant grown in full ms and 1% sucrose, ms25 = plants grown in 25%
815 of full ms) B) Lateral root number and G) primary root length of 18 DAS plants grown in

⁸¹⁶ 30 cm tall cylinders, pots and rhizotrons, all with a volume of 100 cm³ (n = 6-12 plants).
⁸¹⁷ D) Leaf area and E) primary root length of plants of the same age (15 DAS) as the ones
⁸¹⁸ used for the qPCR experiment (n= 6-7). ANOVA analysis with p < 0.01 was used to test
⁸¹⁹ significant differences between the different parameters.



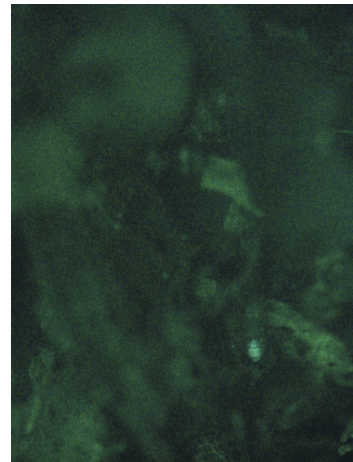
821 *Figure 1-figure supplement 2. PCA plot of shoots of the same samples analyzed in Figure 1.

822 See Figure 1 for more details regarding experimental conditions used.



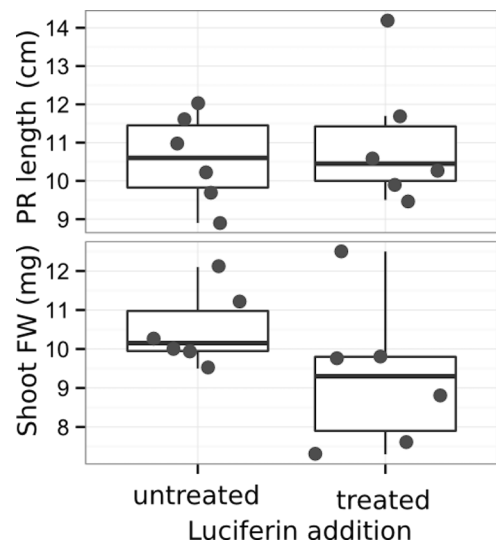
Brightfield

823



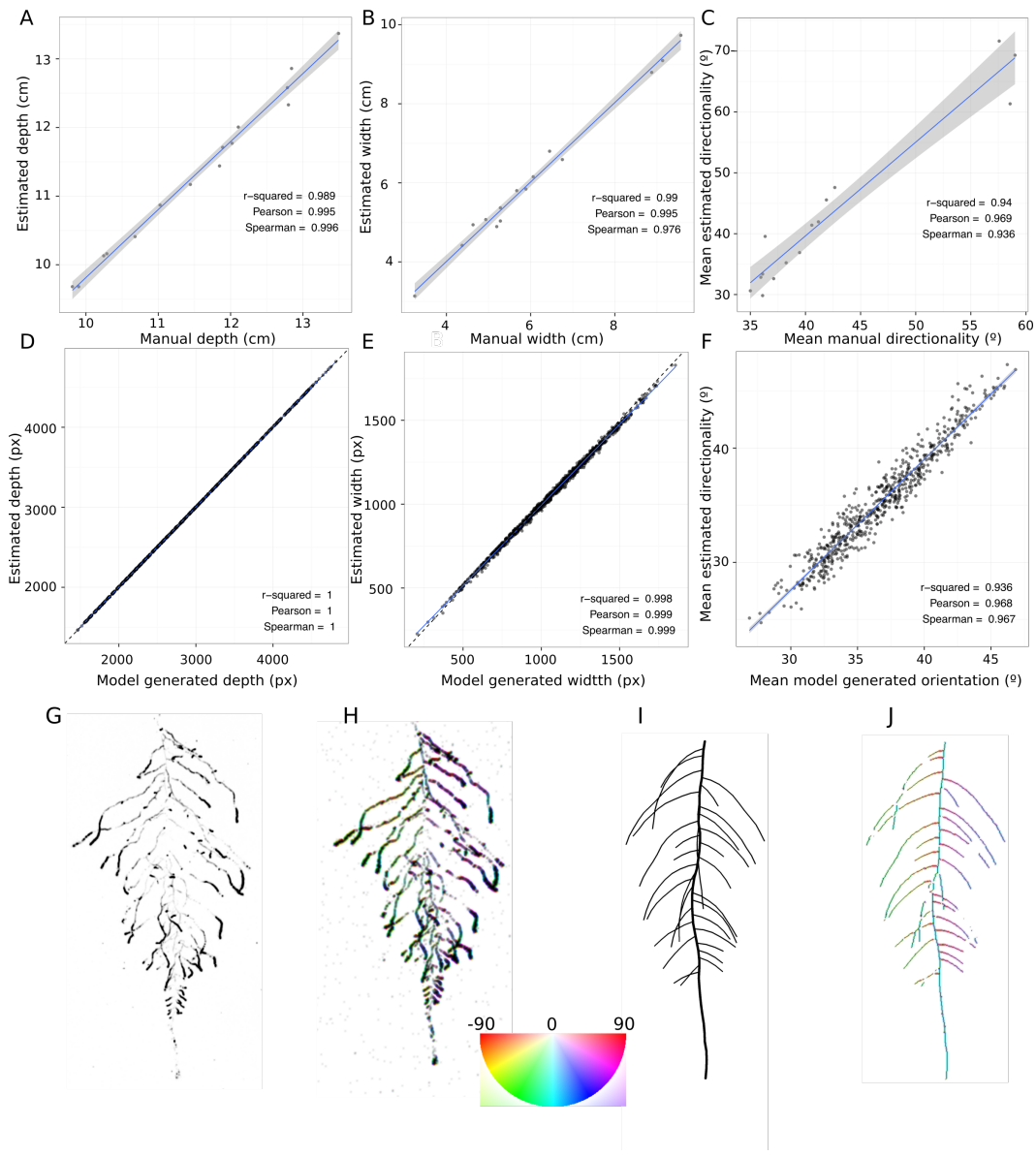
GFP

824 **Figure 1-figure supplement 3** Image of an Arabidopsis root in soil imaged with white
825 light (brightfield) or epifluorescence.



826

827 **Figure 1-figure supplement 4** Effect of luciferin addition on primary root length and
 828 shoot size of 14 DAS seedlings that were either continuously exposed to 300 μ M luciferin
 829 from 9 DAS after sowing or not.

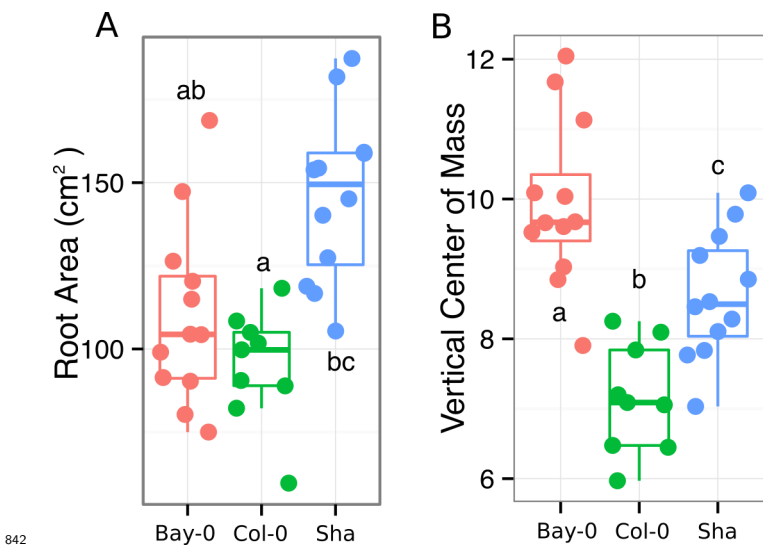


830

831 **Figure 1-figure supplement 5** GLO-RIA ground truth comparison. Tests of GLO-RIA
 832 were performed using two approaches. We first manually quantified root system depth (A)
 833 width (B) and average lateral root angle (C) in a set of 15 root systems corresponding
 834 to different *Arabidopsis* accessions. We also generated 1240 contrasting root systems
 835 using ArchiSimple and quantified root system depth (D) width (E) and directionality
 836 (F) using GLO-RIA. Example of a real (G) and ArchiSimple generated (H) root system

837 and corresponding GLO-RIA determined directionality color-coded into the image (I, J).
838 Absolute orientation angle values are taken before all calculations.

⁸³⁹ **Figure 1-figure supplement data 1:** Two way ANOVA P-values comparing plants grown
⁸⁴⁰ in MS media vs. plants grown in soil (pots or rhizotrons) and plants collected at day or night.
⁸⁴¹ We used p-value < 0.00065 threshold based on Bonferoni adjustment for multiple testing.



843 **Figure 3-figure supplement 1** A) root area, B) vertical center of mass of Bay-0, Col-0
844 and Sha accessions.

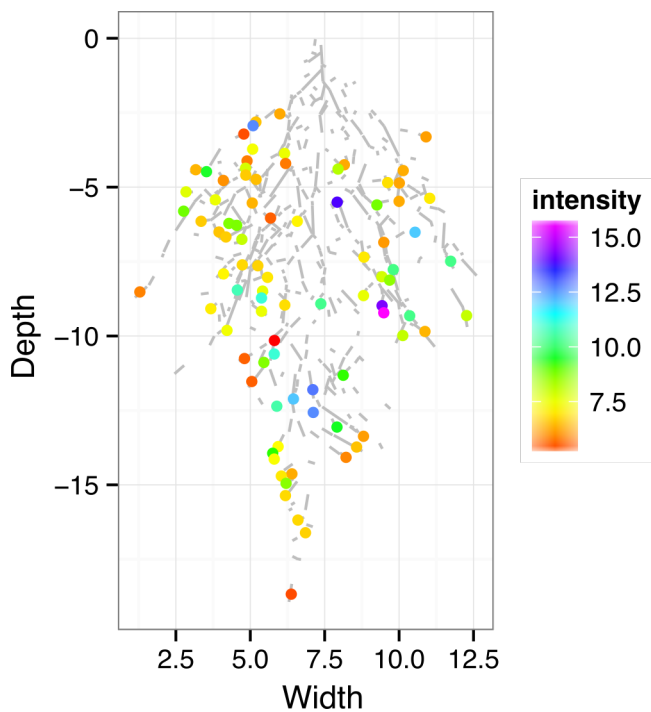
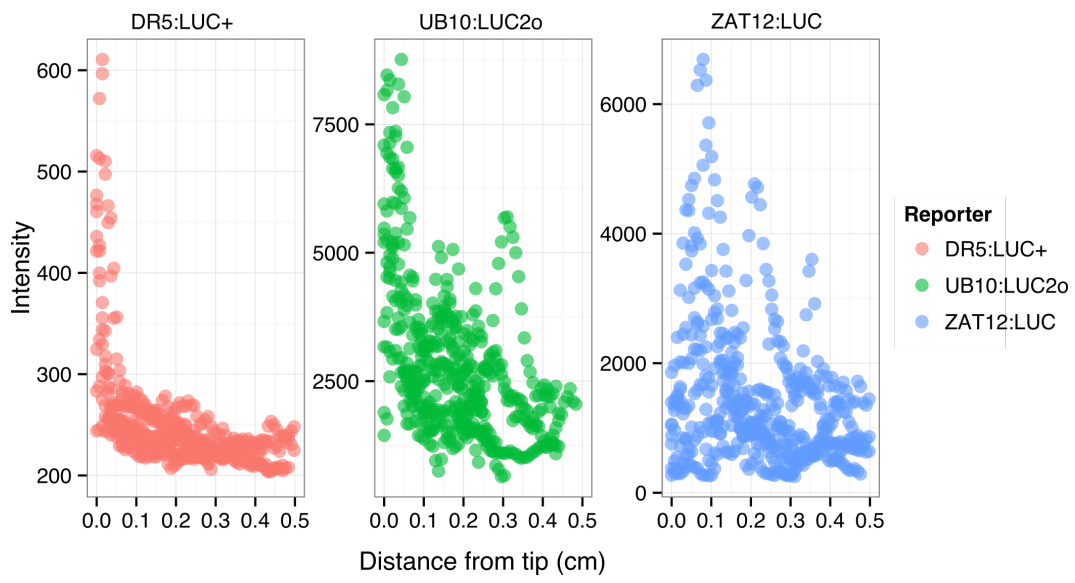


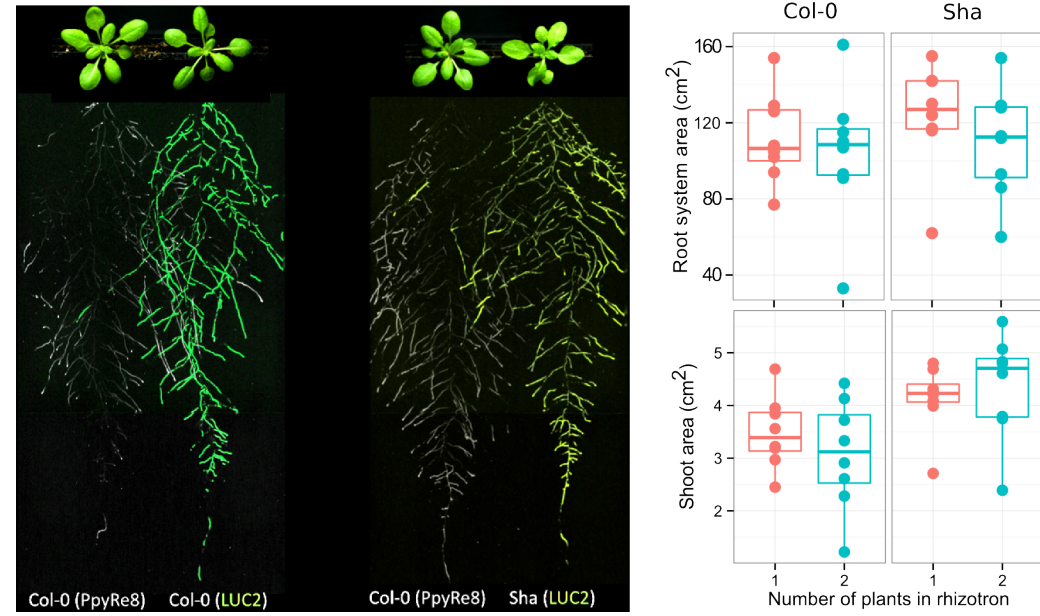
Figure 4-figure supplement 1:

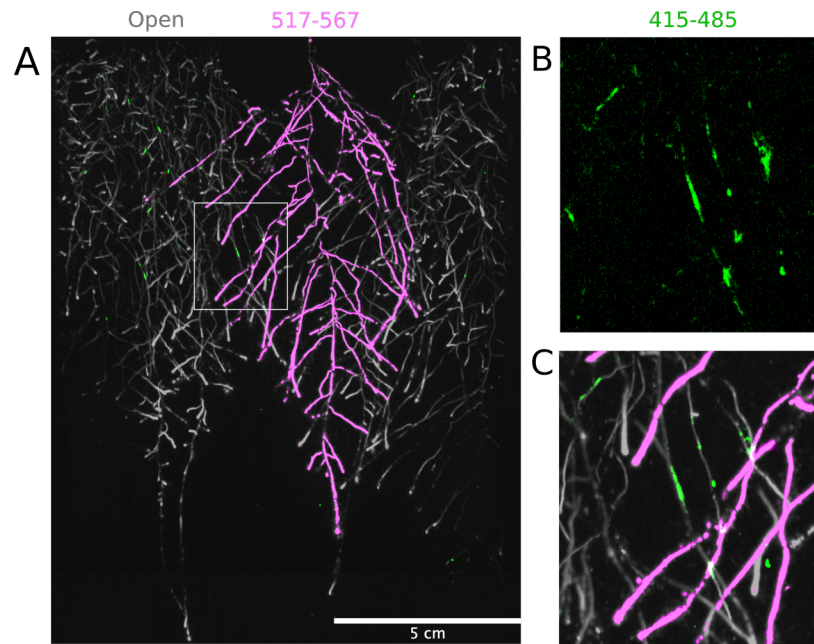
845 ZAT12:LUC intensity and root segments automatically ~~identified values along the root tip.~~
 846 ~~Data was manually obtained by obtaining the intensity profile of the first 0.5 cm from~~
 847 ~~the root tip of individual lateral roots. Ten lateral roots for each reporter were measured.~~
 848 ~~identified with GLO-RIA.~~



851 **Figure 4-figure supplement 2:** DR5:LUC+, UBQ10:LUC2o and ZAT12:LUC intensity
 852 values along the root tip. Data was manually obtained by obtaining the intensity profile
 853 of the first 0.5 cm from the root tip of individual lateral roots. Ten lateral roots for each
 854 reporter were measured.

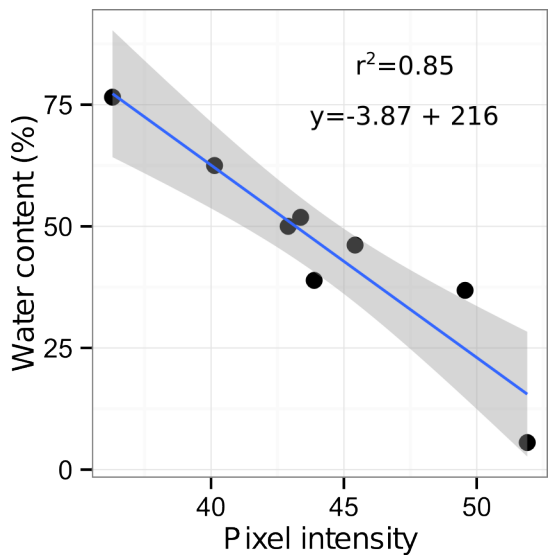
855





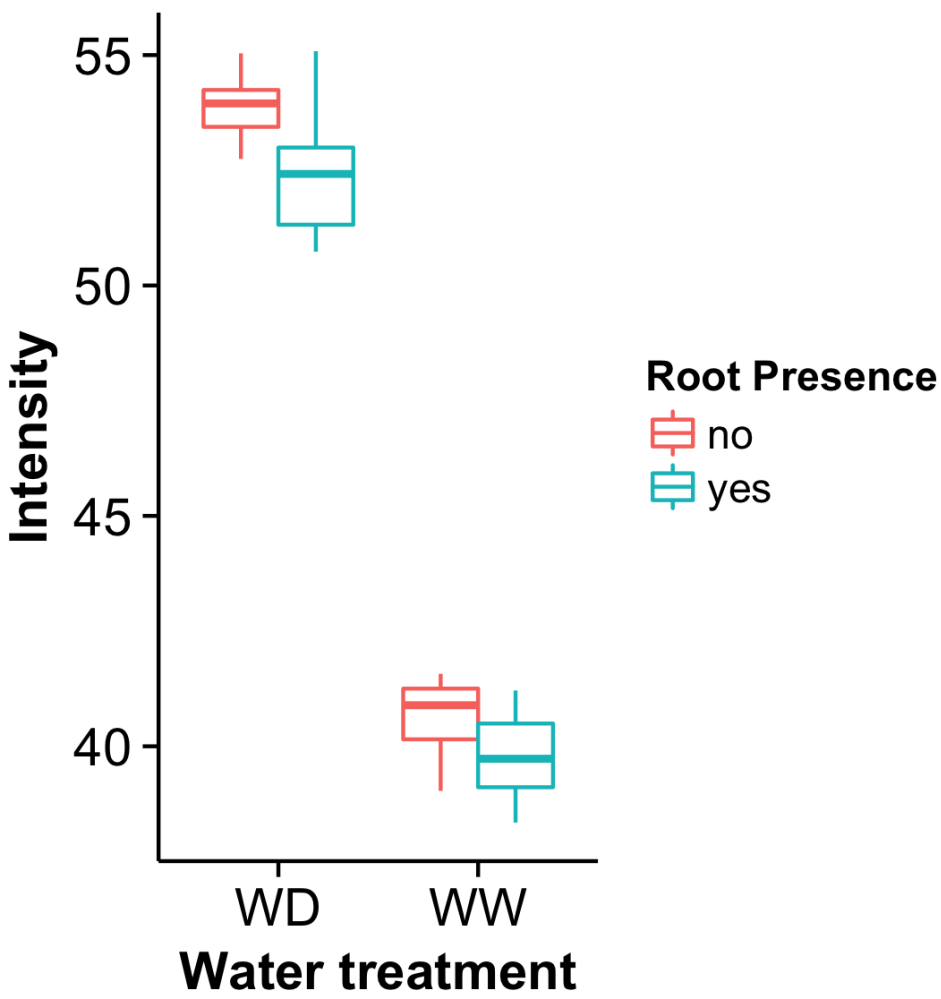
862
 863 **Figure 4-figure supplement 4. Three-reporter-based analysis of root-root-**
 864 **microbe interactions.** A) Image showing a 22 DAS *ProUBQ10:LUC2o* plant (magenta)
 865 grown in the same rhizotron with *ProACT2:PpyRE8o* plants (grey). Plants were inoculated
 866 with *Pseudomonas fluorescens* CH267 (green). Magnified portion of root systems colonized
 867 by *Pseudomonas fluorescens* showing *P. fluorescences* (B) only or all three reporters together
 868 (C).

869



870 **Figure 5-figure supplement 1:** Moisture calibration curve. Rhizotrons with different
871 levels of moisture were prepared and scanned to obtain readings of pixel intensity. Soil from
872 rhizotrons was then weighed, dried down in an oven at 70 °C for 48 hours and percent water
873 content quantified.
874

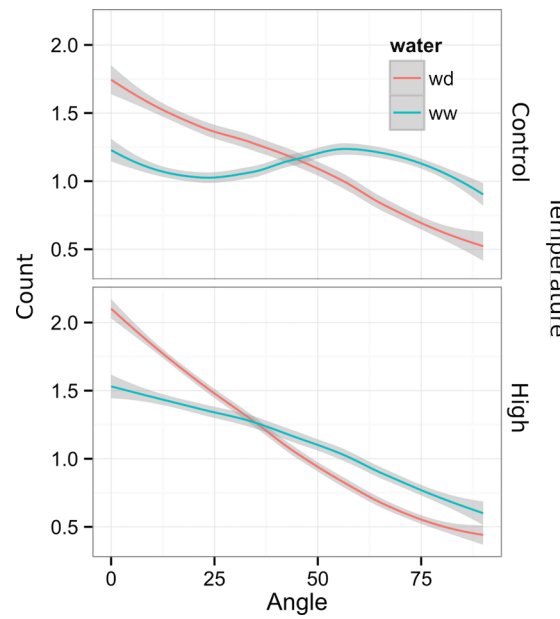
875



876

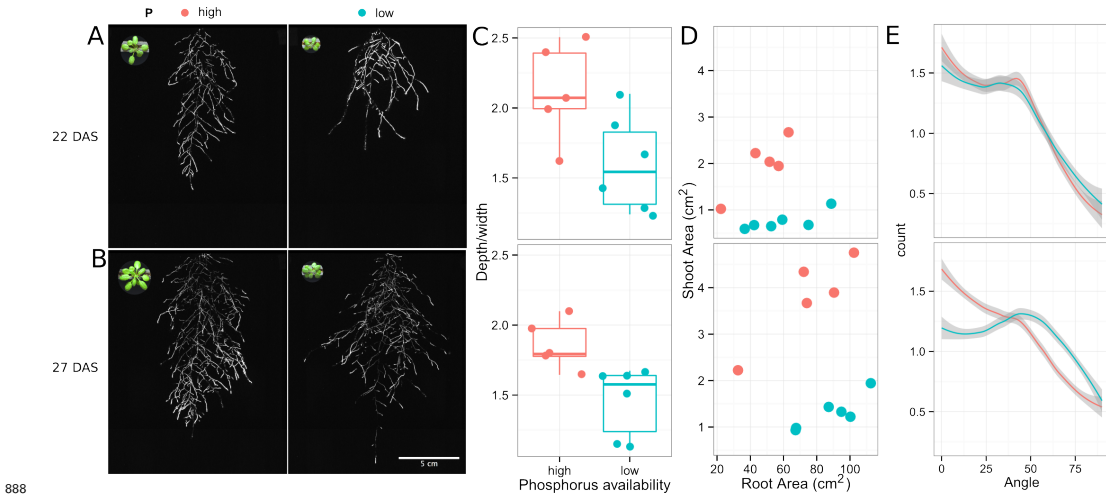
877 **Figure 5-figure supplement 2.** Comparison of soil intensity values between
 878 **areas of the rhizotron with or without the presence of roots, determined based**
 879 **on luminescence data.** Mean intensity values from 100 x 100 pixel squares samples of
 880 both areas were obtained from 10 different rhizotrons. Wilcoxon test analysis with $p < 0.01$
 881 was used to test significant differences between areas with our without root presence.

882



883
884 **Figure 6-figure supplement 1** Directionality analysis of roots of plants transferred to
885 water deprivation conditions after 9 DAS and kept 22 °C (control temperature) and 29 °C
886 (high temperature) until 22 DAS. (0° is the direction of the gravity vector).

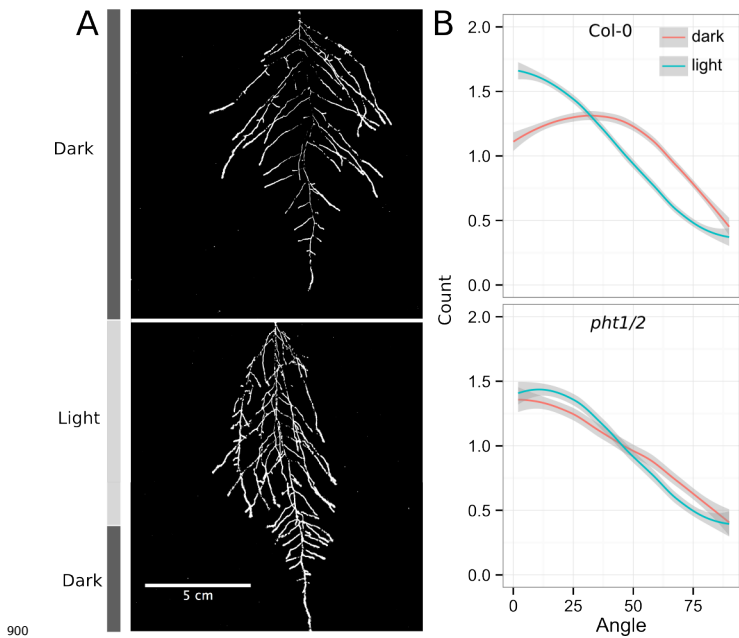
887



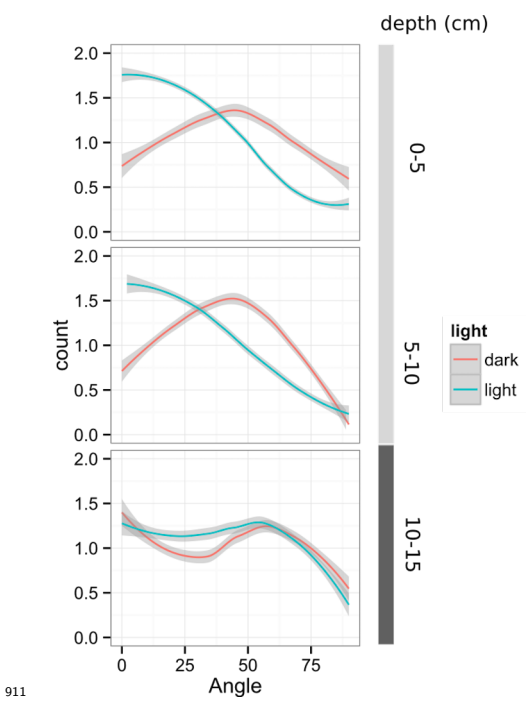
889 **Figure 6-figure supplement 2. Phosphorus deficiency response of root systems**

890 Shoot and root systems of *ProUBQ10:LUC2o* Col-0 plants growing in soil supplemented
 891 with 1ml of 100 μ M P-Alumina (left) and 0-P-Alumina (right) 22 (A) or 27 (B) DAS. C)
 892 Root depth/width ratio of 22 (top) and 27 (bottom) DAS plants. D) Scatter-plot showing
 893 relationship between root and shoot system area at 22 (top) and 27 (bottom) DAS. E) Root
 894 directionality distribution in plants 22 (top) and 27 (bottom) DAS. Anova analysis at $p <$
 895 0.01 was used to compare depth/width ratios in P treatments. Kolmogorov-Smirnov test at
 896 $p < 0.001$ was used to compare directionality distributions between the different treatments.
 897 A Local Polynomial Regression Fitting with 95% confidence interval (grey) was used to
 898 represent the directionality distribution curve.(0° is the direction of the gravity vector).

899

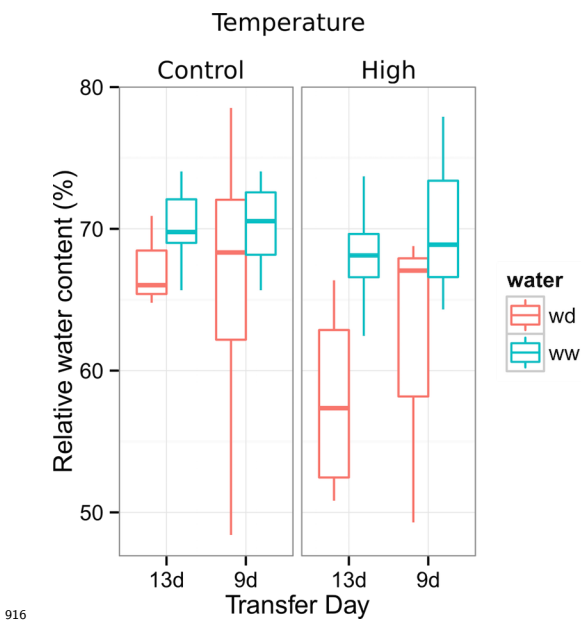


901 **Figure 6-figure supplement 3. Effect of light on root directionality.** A) Col-0 root
902 systems shielded (top) or light exposed (bottom). After 9 DAS the top third of the rhizotron
903 was exposed to light (indicated on the side with a light grey bar) and plants were imaged
904 at 20 DAS. B) Directionality analysis of root systems shielded (red) or exposed (green) to
905 light for Col-0 (top panel) or *pht1/2* double mutant (bottom panel). Between 4 and 6
906 plants were analyzed per treatment. ANOVA analysis at $p < 0.01$ was used to compare
907 depth/width ratios in P treatments. Kolmogorov-Smirnov test at $p < 0.001$ was used to
908 compare directionality distributions between the different treatments. A Local Polynomial
909 Regression Fitting with 95% confidence interval (grey) was used to represent the directionality
910 distribution curve.(0° is the direction of the gravity vector).

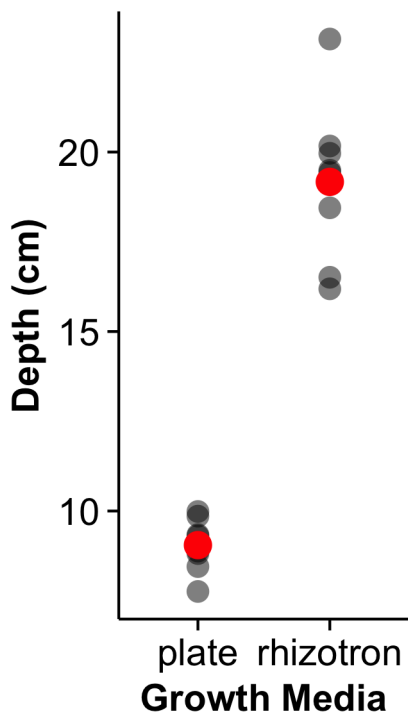


911 **Figure 6-figure supplement 4** Plots showing output of directionality analysis performed
 912 at different depths (0-5, 5-10, 10-15 cm) in rhizotrons exposed to light or kept in the dark.
 913
 914 (0° is the direction of the gravity vector).

915



916 **Figure 6-figure supplement 5.** Leaf relative water content of 23 DAS plants that
 917 were subjected to water deprivation (WD) after 9 or 13 DAS or kept under
 918 well watered (WD) conditions. At 9 DAS half of the plants were kept under control
 919 temperature conditions (22 °C) and the other half transferred to a 29 °C (high) chamber. n
 920 = 6-8 plants.
 921
 922



923

924 **Figure 8-figure supplement 1** Depth of the primary root of *Brachypodium* plants grown

925 in rhizotrons or on gel-based media (n=8-11). [Red dots indicate mean values.](#)

926

927 **Supplementary material**

928 **Supplemental Material 1**

929 Blueprints of the holders, clear sheets and spacers needed to built the rhizotrons. Additional
930 details are provided in the materials and methods. Files are provided in Adobe Illustrator
931 .ai and Autocad .dxf formats.

932 **Supplemental Material 2**

933 Primers used in the qPCR experiment.

934 **Supplemental Material 3**

935 Vector maps of all the constructs used in this work.

936 **Source data files**

937 Source data files used for building the following figures are provided:

938 [figure.csv](#)Figure 1-source data 1

939 [figure-B.csv](#)Figure 1-figure supplement 1-source data 1

940 [figure.csv](#)Figure 1-figure supplement 2-source data 1

941 [figure-F.csv](#)Figure 1-figure supplement 3-source data 1

942 [figure.csv](#)Figure 1-figure supplement 5-source data 1

943 [figure.csv](#)Figure 2-source data 1

944 [figure.csv](#)Figure 3-source data 1

945 [figure.csv](#)Figure 3-source data 2

946 [figure.csv](#)Figure 3-figure supplement 1-source data 1

947 [figure.csv](#)Figure 4-source data

948 [figure-G.csv](#)Figure 4-figure supplement 1-source data 1

949 [figure-G.tps](#)Figure 4-figure supplement 2-source data 1

950 [figure-B.csv](#)Figure 5-figure supplement 1-source data 1

951 [figure.csv](#)figure.csvfigure.csvfigure.csvfigure_5_figure_supplement_1.csv

952 [figure-D.csv](#)Figure 6-source data 1

953 [figure-C-D.csv](#)Figure 6-figure supplement 2-source data 1
954 [figure-E.csv](#)Figure 6-figure supplement 3-source data 1
955 [figure.csv](#)Figure 6-figure supplement 4-source data 1
956 [figure.csv](#)Figure 6-figure supplement 5-source data 1
957 [figure.csv](#)Figure 7-source data 1
958 [figure.csv](#)[figure.csv](#)Figure 8-figure supplement 1-source data 1

959

960 **References**

- 961 1.Dinneny, J. R. *et al.* Cell identity mediates the response of *Arabidopsis* roots to abiotic
962 stress. *Science* **320**, 942–945 (2008).
- 963 2.Duan, L. *et al.* Endodermal ABA Signaling Promotes Lateral Root Quiescence during Salt
964 Stress in Arabidopsis Seedlings. *Plant Cell* **25**, 324–341 (2013).
- 965 3.Lynch, J. P. & Wojciechowski, T. Opportunities and challenges in the subsoil: pathways to
966 deeper rooted crops. *J. Exp. Bot.* **66**, 2199–2210 (2015).
- 967 4.Brady, N. C. & Weil, R. R. *Elements of the nature and properties of soils*. (Prentice Hall,
968 2009).
- 969 5.Bao, Y. *et al.* Plant roots use a patterning mechanism to position lateral root branches
970 toward available water. *Proc Natl Acad Sci* **111**, 9319–9324 (2014).
- 971 6.Tabata, R. *et al.* Perception of root-derived peptides by shoot LRR-RKs mediates systemic
972 N-demand signaling. *Science* **346**, 343–346 (2014).
- 973 7.Rosquete, M. R. *et al.* An Auxin Transport Mechanism Restricts Positive Orthogravitropism
974 in Lateral Roots. *Current Biology* **23**, 817–822 (2013).
- 975 8.Uga, Y. *et al.* Control of root system architecture by DEEPER ROOTING 1 increases rice
976 yield under drought conditions. *Nat. Genet.* **45**, 1097–1102 (2013).
- 977 9.Postma, J. A. & Lynch, J. P. The optimal lateral root branching density for maize depends
978 on nitrogen and phosphorus availability. *Plant Physiol.* **166**, 590–602 (2014).
- 979 10.[Laliberté, E. *et al.* How does pedogenesis drive plant diversity? *Trends in ecology & evolution* **28**, 331–340 \(2013\).](#)
- 981 11.[Tian, H., De Smet, I. & Ding, Z. Shaping a root system: regulating lateral versus primary
982 root growth. *Trends in plant science* **19**, 426–431 \(2014\).](#)
- 983 12.[Schneider, C. A., Rasband, W. S. & Eliceiri, K. W. NIH Image to ImageJ: 25 years of
984 image analysis. *Nature methods* **9**, 671–675 \(2012\).](#)

- 985 11.13. Meijon, M., Satbhai, S. B., Tsuchimatsu, T. & Busch, W. Genome-wide association
986 study using cellular traits identifies a new regulator of root development in. *Nat. Genet.*
987 **46**, 77–81 (2013).
- 988 12.14. Hall, M. P. *et al.* Engineered Luciferase Reporter from a Deep Sea Shrimp Utilizing
989 a Novel Imidazopyrazinone Substrate. *ACS chemical biology* **7**, 1848–1857 (2012).
- 990 15. Hara-Miyauchi, C. *et al.* Bioluminescent system for dynamic imaging of cell and animal
991 behavior. *Biochem. Biophys. Res. Commun.* **419**, 188–193 (2012).
- 992 13.16. Emami, S., Yee, M.-C. & Dinneny, J. R. A robust family of Golden Gate Agrobacterium
993 vectors for plant synthetic biology. *Front. Plant Sc.* **4**, 339 (2013).
- 994 14. Hall, M. P. *et al.* Engineered Luciferase Reporter from a Deep Sea Shrimp Utilizing a
995 Novel Imidazopyrazinone Substrate. *ACS chemical biology* **7**, 1848–1857 (2012).
- 996 15.17. Ristova, D. *et al.* RootScape: a landmark-based system for rapid screening of root
997 architecture in Arabidopsis. *Plant Physiology* **161**, 1086–1096 (2013).
- 998 16.18. Lobet, G. *et al.* Root System Markup Language: toward a unified root architecture
999 description language. *Plant Physiol.* **167**, 617–627 (2015).
- 1000 17.19. Pagès, L. *et al.* Calibration and evaluation of ArchiSimple, a simple model of root
1001 system architecture. *Ecological Modelling* **290**, 76–84 (2014).
- 1002 20. Moreno-Risueno, M. A. *et al.* Oscillating gene expression determines competence for
1003 periodic *Arabidopsis* root branching. *Science* **329**, 1306–1311 (2010).
- 1004 18.21. Miller, G. *et al.* The plant NADPH oxidase RBOHD mediates rapid systemic signaling
1005 in response to diverse stimuli. *Science Signaling* **2**, ra45 (2009).
- 1006 19.22. Haney, C. H., Samuel, B. S., Bush, J. & Ausubel, F. M. Associations with rhizosphere
1007 bacteria can confer an adaptive advantage to plants. *Nature Plants* **1**, 15051 (2015).
- 1008 20.23. Mandoli, D. F., FORD, G. A., WALDRON, L. J., NEMSON, J. A. & Briggs, W. R.
1009 Some spectral properties of several soil types: implications for photomorphogenesis*. *Plant
1010 Cell Environ.* **13**, 287–294 (1990).

- 1011 21.24. Galen, C., Rabenold, J. J. & Liscum, E. Functional ecology of a blue light photoreceptor:
1012 effects of phototropin-1 on root growth enhance drought tolerance in *Arabidopsis thaliana*.
1013 *New Phytol.* **173**, 91–99 (2007).
- 1014 22.25. Moni, A., Lee, A. Y., Briggs, W. R. & Han, I. S. The blue light receptor Phototropin 1
1015 suppresses lateral root growth by controlling cell elongation. *Plant Biology* 34–40 (2014).
- 1016 23.26. Yokawa, K., Kagenishi, T. & Baluška, F. Root photomorphogenesis in laboratory-
1017 maintained *Arabidopsis* seedlings. *Trends Plant Sci.* **18**, 117–119 (2013).
- 1018 24.27. Lobell, D. B. *et al.* Greater Sensitivity to Drought Accompanies Maize Yield Increase
1019 in the U.S. Midwest. *Science* **344**, 516–519 (2014).
- 1020 25.28. Ort, D. R. & Long, S. P. Limits on Yields in the Corn Belt. *Science* **344**, 484–485
1021 (2014).
- 1022 26.29. Pacheco-Villalobos, D. & Hardtke, C. S. Natural genetic variation of root system
1023 architecture from *Arabidopsis* to *Brachypodium*: towards adaptive value. *Philosophical
1024 Transactions of the Royal Society of London B: Biological Sciences* **367**, 1552–1558 (2012).
- 1025 27.30. Watt, M., Schneebeeli, K., Dong, P. & Wilson, I. W. The shoot and root growth of
1026 *Brachypodium* and its potential as a model for wheat and other cereal crops. *Functional
1027 Plant Biol.* **36**, 960–969 (2009).
- 1028 28.31. Mann, D. G. J. *et al.* Gateway-compatible vectors for high-throughput gene functional
1029 analysis in switchgrass (*Panicum virgatum* L.) and other monocot species. *Plant Biotechnol.
1030 J.* **10**, 226–236 (2012).
- 1031 29.32. Pacheco-Villalobos, D., Sankar, M., Ljung, K. & Hardtke, C. S. Disturbed Local Auxin
1032 Homeostasis Enhances Cellular Anisotropy and Reveals Alternative Wiring of Auxin-ethylene
1033 Crosstalk in *Brachypodium distachyon* Seminal Roots. *PLoS Genet* **9**, e1003564 (2013).
- 1034 30.33. Buer, C. S., Wasteneys, G. O. & Masle, J. Ethylene modulates root-wave responses in
1035 *Arabidopsis*. *Plant Physiology* **132**, 1085–1096 (2003).
- 1036 31.34. Blossfeld, S., Schreiber, C. M., Liebsch, G., Kuhn, A. J. & Hinsinger, P. Quantitative

- 1037 imaging of rhizosphere pH and CO₂ dynamics with planar optodes. *Annals of Botany* **112**,
1038 267–276 (2013).
- 1039 **32.35.** Shaw, S. L. & Ehrhardt, D. W. Smaller, Faster, Brighter: Advances in Optical Imaging
1040 of Living Plant Cells. *Annu. Rev. Plant Biol.* **64**, 351–375 (2013).
- 1041 **33.36.** Barr, H. & Weatherley, P. A re-examination of the relative turgidity technique for
1042 estimating water deficit in leaves. *Aust. J. Biol. Sci* **15**, 413–428 (1962).
- 1043 **34.37.** Grapov, D. DeviumWeb: Dynamic Multivariate Data Analysis and Visualization
1044 Platform.
- 1045 **35.38.** Branchini, B. R. *et al.* Red-emitting luciferases for bioluminescence reporter and
1046 imaging applications. *Analytical Biochemistry* **396**, 290–297 (2010).
- 1047 **36.39.** Branchini, B. R. *et al.* Thermostable red and green light-producing firefly luciferase
1048 mutants for bioluminescent reporter applications. *Analytical Biochemistry* **361**, 253–262
1049 (2007).
- 1050 **37.40.** Lane, M. C., Alteri, C. J., Smith, S. N. & Mobley, H. L. T. Expression of flagella is
1051 coincident with uropathogenic Escherichia coli ascension to the upper urinary tract. *Proc.
1052 Natl. Acad. Sci. U.S.A.* **104**, 16669–16674 (2007).
- 1053 **38.41.** Ruegger, M. *et al.* The TIR1 protein of Arabidopsis functions in auxin response and is
1054 related to human SKP2 and yeast grr1p. *Genes Dev* **12**, 198–207 (1998).
- 1055 **39.42.** Moriwaki, T. *et al.* Hormonal Regulation of Lateral Root Development in Arabidopsis
1056 Modulated by MIZ1 and Requirement of GNOM Activity for MIZ1 Function. *Plant Physiol.*
1057 **157**, 1209–1220 (2011).
- 1058 **40.43.** Vogel, J. & Hill, T. High-efficiency Agrobacterium-mediated transformation of Brachy-
1059 podium distachyon inbred line Bd21-3. *Plant Cell Rep* **27**, 471–478 (2008).
- 1060 **41.44.** Covington, M. F. & Harmer, S. L. The Circadian Clock Regulates Auxin Signaling
1061 and Responses in Arabidopsis. *Plos Biol* **5**, e222 (2007).

- 1062 42.45 Lindeboom, J. J. *et al.* A Mechanism for Reorientation of Cortical Microtubule Arrays
1063 Driven by Microtubule Severing. *Science* **342**, 1245533–1–1245533–11 (2013).
- 1064 43.46 Chitwood, D. H. *et al.* A modern ampelography: a genetic basis for leaf shape and
1065 venation patterning in grape. *Plant Physiology* **164**, 259–272 (2014).
- 1066 44.47 Iwata, H. & Ukai, Y. SHAPE: a computer program package for quantitative evaluation
1067 of biological shapes based on elliptic Fourier descriptors. *The Journal of Heredity* **93**, 384–385
1068 (2002).
- 1069 45.48 R Core Team. *R: A language and environment for statistical computing*. (R Foundation
1070 for Statistical Computing, 2014). at <<http://www.R-project.org/>>
- 1071 46.49 Wickham, H. *Tidyr: Easily tidy data with spread() and gather() functions*. (2014). at
1072 <<http://CRAN.R-project.org/package=tidyr>>
- 1073 47.50 Auguie, B. *GridExtra: Functions in grid graphics*. (2012). at <<http://CRAN.R-project.org/package=gridExtra>>
- 1074 48.51 Dryden, I. L. *Shapes: Statistical shape analysis*. (2013). at <<http://CRAN.R-project.org/package=shapes>>
- 1075 49.52 Adams, D. & Otarola-Castillo, E. Geomorph: An r package for the collection and
1076 analysis of geometric morphometric shape data. *Methods in Ecology and Evolution* **4**, 393–399
1077 (2013).
- 1078 50.53 Wickham, H. *Ggplot2: Elegant graphics for data analysis*. (Springer New York, 2009).
1079 at <<http://had.co.nz/ggplot2/book>>
- 1080 51.54 Wilke, C. O. *cowplot: Streamlined Plot Theme and Plot Annotations for ggplot2*. (2015).
1081 at <<http://cran.r-project.org/web/packages/cowplot/index.html>>